J. Fluid Mech. (1995), *vol.* 287, *pp.* 317–348

Regeneration mechanisms of near-wall turbulence structures

By JAMES M. HAMILTON†, JOHN KIM‡, AND FABIAN WALEFFE¶

Center for Turbulence Research, Stanford University, Stanford, CA 94305
and NASA-Ames Research Center, MS 202A-1, Moffett Field, CA 94035, USA

(Received 18 February 1994 and in revised form 27 October 1994)

Direct numerical simulations of a highly constrained plane Couette flow are employed to study the dynamics of the structures found in the near-wall region of turbulent flows. Starting from a fully developed turbulent flow, the dimensions of the computational domain are reduced to near the minimum values which will sustain turbulence. A remarkably well-defined, quasi-cyclic and spatially organized process of regeneration of near-wall structures is observed. This process is composed of three distinct phases: formation of streaks by streamwise vortices, breakdown of the streaks, and regeneration of the streamwise vortices. Each phase sets the stage for the next, and these processes are analysed in detail. The most novel results concern vortex regeneration, which is found to be a direct result of the breakdown of streaks that were originally formed by the vortices, and particular emphasis is placed on this process. The spanwise width of the computational domain corresponds closely to the typically observed spanwise spacing of near-wall streaks. When the width of the domain is further reduced, turbulence is no longer sustained. It is suggested that the observed spacing arises because the time scales of streak formation, breakdown and vortex regeneration become mismatched when the streak spacing is too small, and the regeneration cycle at that scale is broken.

1. Introduction

One of the remarkable features of the coherent structures observed in turbulent shear flows is that these structures are self-regenerating. Though individual structures may break up or decay, their presence ensures the creation of subsequent structures. It is through a continuous cycle of generation and regeneration that the turbulence is sustained. In the near-wall region, the predominant structures are low- and high-speed streaks and streamwise vortices, and these structures have a characteristic spanwise 'wavelength', widely observed (Kline *et al.* 1967; Smith & Metzler 1983; Kim, *et al.* (1987) to be about 100 ν/u_τ (where $u_\tau = (\tau_w/\rho)^{1/2}$ is the friction velocity, τ_w is the shear stress at the wall, ρ is the density, and ν is the kinematic viscosity). After much study, the kinematics of coherent structures have been well characterized

† Present address: Molecular Devices Corp., 1311 Orleans Drive, Sunnyvale, CA 94089, USA.
‡ Present address: Mechanical, Aerospace and Nuclear Engineering Department, University of California, Los Angeles, 405 Hilgard Avenue, Los Angeles, CA 90024-1597, USA.
¶ Present address: Department of Mathematics, Room 2-378, Massachusetts Institute of Technology, Cambridge, MA 02139, USA.

(e.g. Kline *et al.* 1967; Robinson 1991), but the dynamics of the various mechanisms involved in the regeneration process, including the factors which govern the spanwise spacing of the streaks, have proven tremendously difficult to ascertain. Direct examination of the flow dynamics in a fully turbulent flow is complicated by the random distribution of the coherent structures in space and time, by the fact that no two realizations of a structure are identical, and by the presence of additional structures ('debris') which may not be necessary components of the regeneration process.

Several investigators have sidestepped these complications by studying simplified flows and, often, by considering only part of the regeneration process. In each case, the goal has been to reduce the complexity of the problem while preserving the essential dynamics under investigation. Jiménez & Moin (1991) used direct numerical simulation to study turbulence in a channel flow at Reynolds numbers of 2000 to 5000. Simplification was achieved by considering a computational domain in which the streamwise and spanwise dimensions were near the minimum values required to sustain turbulence. The boundary conditions in these directions were periodic, and the simulated flow thus consisted of a periodic array of identical cells. Despite the constraint imposed by the small size of the computational domain, various statistical measures (mean streamwise velocity profile, Reynolds stresses, turbulence intensities) and turbulence structures (sublayer streaks, streamwise vortices, near-wall shear layers) in the near-wall region closely matched those observed by other investigators. Sendstad & Moin (1992) also used this technique to study the dynamics of near-wall structures. Aubry *et al.* (1988) used a dynamical systems approach to study the behaviour of streamwise vortices in the near-wall region of turbulent boundary layers. They were able to achieve a great reduction in the complexity of the observed flow by using a severely truncated modal decomposition and by considering only the region very near the wall. Intermittent behaviour of the streamwise vortices, similar to the bursting events widely observed in the near-wall region, was reproduced and studied. No attempt was made, however, to recreate the full regeneration cycle: the origin of the streamwise vortices, including the possible role of the bursting events in producing these vortices, was outside the scope of the study.

The origin of the streamwise vortices was addressed by Jang, Benney & Gran (1986) who employed 'direct resonance' theory to explain the observed spanwise spacing of the vortices and the accompanying streaks. The direct resonance mechanism produces rapid growth of oblique wall-normal vorticity modes, but applies only to modes which satisfy a resonance condition, and thus provides a scale selectivity. These wall-normal vorticity modes can then interact nonlinearly to form streamwise vortices and streaks of the correct spacing. Subsequently, however, Waleffe, Kim & Hamilton (1993) examined direct resonance and noted that some non-resonant modes were amplified more than the resonant modes, eliminating any scale selection due to the resonance mechanism. Furthermore, they found that the creation of streamwise vortices by the interactions of oblique modes was dominated by the interactions of the wall-normal velocity modes, rather than the wall-normal vorticity modes as required for scale selection in the direct resonance theory.

Waleffe *et al.* (1993) also examined the possibility that the spanwise spacing of the streaks is determined by a length scale associated with the mean velocity profile of the turbulent flow. The streamwise vortices are found very near the wall where the velocity gradient is highest, and it is reasonable to imagine that a streak spacing proportional to the thickness of the high-gradient layer is favoured (selective amplification). This was found not to be the case, however, as the peak in wall-normal vorticity response is too weak to be significant, and, in any case, corresponds to a streak spacing of

less than half the observed value. Thus, neither of the linear mechanisms (direct resonance and selective amplification) studied by Waleffe *et al.* was found to explain the spanwise spacing of streaks.

Butler & Farrell (1993) employed a variational approach to find 'optimal' perturbations – perturbations that produce the greatest growth in perturbation energy over a given time – and applied this technique to study streak spacing. They found that streamwise vortices are the optimal perturbations in a flow with a characteristically turbulent mean velocity profile, and that when the optimization is constrained by a time scale (eddy turnover time) imposed by the turbulence, these vortices produce streaks with the correct spacing. The optimal perturbation mechanism is linear, but the processes which govern the eddy turnover time are nonlinear. No generation mechanism is described for the optimal streamwise vortices, and it is supposed that the near-wall region contains streamwise vortices of many sizes with only those of the optimal size producing energetic streaks within the allowed time. Other evidence, however, suggests that this is not the case. Robinson (1991), for instance, reports a sharp peak in the distribution of streamwise vortex diameters, with 73% of the visually identified streamwise vortices in a numerically simulated turbulent boundary layer having diameters of 10 – 40 viscous lengths.

Jiménez & Moin (1991) addressed the issue of streak spacing when they noted that turbulence could not be sustained in their plane channel flow simulations if the spanwise dimension of the computational domain was less than the normally observed streak spacing of about 100 wall units, even though the flow Reynolds number, based on half the separation of the channel walls, was 2000 to 5000. This is a fascinating result since reducing the width not only eliminated the streaks, but the turbulence too. The streaks (or whatever produces them) are not mere artifacts, but essential features of turbulent flow. Waleffe *et al.* observed that at 100 wall units, the width of the channel is much less than the wall separation, and that the Reynolds number might more appropriately be based on the spanwise dimension. Indeed, the characteristic spanwise spacing, λ_z, when expressed in wall units, $u_\tau \lambda_z / \nu$, is a Reynolds number and the value of 100 may best be regarded as the critical Reynolds number for sustained turbulence. Waleffe *et al.* conjectured that the preferred spanwise spacing, the critical Reynolds number, is set by the entire process of self-regeneration, rather than by any of the individual mechanisms that constitute the process. Hence the failure of the linear approaches which attempted to analyse only a single mechanism (e.g. streak formation). Waleffe *et al.* went on to show that the critical Reynolds number obtained from the streak spacing, after conversion to the conventional flow Reynolds number, gives the correct critical values for plane Poiseuille, plane Couette, and other shear flows. This suggests that 100 may be a universal critical Reynolds number for near-wall processes.

Another approach to understanding turbulence regeneration is to assemble various known dynamical processes into a 'conceptual model' of the regeneration cycle. A plausible model must accurately reproduce the observed behaviour of turbulence structures and should include some sort of feedback mechanism to close the cycle. One such model of the near-wall region is due to Jiménez (1994). In his model lateral instability waves form in regions of large wall-normal vorticity that separate the streaks. Streamwise vortices form as this vorticity is tilted into the streamwise direction by the shearing action of the mean flow. He goes on to show that the characteristic spanwise spacing of the streaks can be estimated from the wavelength of the lateral instability waves and a balance of vortex concentration by stretching versus viscous diffusion. The cycle is closed with the formation of new streaks by

the streamwise vortices. A different mechanism for streamwise vortex generation is proposed in the conceptual model of Sreenivasan (1988). He adopts the idea of Coles (1978) that the streamwise vortices arise through a Görtler, or centrifugal, instability mechanism. This mechanism is driven by near-wall pathlines that have concave-upward curvature as a result of some large-scale disturbance. A closely related phenomenon is the Craik–Leibovich instability (Craik & Leibovich 1976). The original analysis for the Craik–Leibovich instability was developed in connection with Langmuir circulations, arrays of vortices aligned with the wind direction found near the surface in oceans and lakes. The Craik–Leibovich instability mechanism has also been proposed as the source of streamwise vorticity in the near-wall region of turbulent flows, and Craik (1982) has provided an Eulerian interpretation of the instability showing it to be very similar to the Görtler instability mechanism.

Clearly, there is no shortage of reasonable candidate mechanisms for the regeneration of near-wall structures, but the complications of turbulent flow make narrowing down the list very difficult. In the present study, we begin with a turbulent plane Couette flow and progressively reduce the Reynolds number and dimensions of the computational domain to near the minimum values for which turbulence can be sustained. The complexity of the resulting flow is greatly reduced, yet the essential dynamics of the regeneration cycle are retained. This is in contrast to the more common approach in transition and turbulence studies of considering deterministic perturbations to a laminar or mean shear flow. One advantage of our minimal turbulent flow is that it allows us to examine the regeneration cycle as a whole, and to evaluate each phase of regeneration in the context of the others to provide a complete and consistent description of the entire cycle.

The approach used in the present study is similar to that of Jiménez & Moin (1991) in the reduction of the streamwise and spanwise extent of the computational domain, but here the constraints imposed on the flow are much stronger. They examined a channel flow of low to moderate Reynolds number while the present flow is a plane Couette flow of minimal Reynolds number. The mean flow in a channel has shear of opposite sign at each wall and therefore two separate near-wall regions. Plane Couette flow has a single-signed shear and, as will be seen, at low Reynolds numbers the two walls share a single set of structures.

The direct numerical simulation technique and flow geometry used in the present study are presented in §2 of this paper. The general characteristics of the regeneration cycle are discussed in §3. This is followed by an examination of the various phases of regeneration, with streak formation in §4, streak breakdown in §5, and streamwise vortex regeneration in §6. In §7, streak spacing is considered in the context of the regeneration mechanism. The results of the present study are compared to those of previous investigations in §8, and both similarities and differences are noted.

2. Numerical method and flow geometry

The direct numerical simulation results presented in this paper were obtained using the pseudo-spectral channel flow code of Kim, *et al.* (1987) modified to simulate plane Couette flow and using a third-order Runge–Kutta time advancement for the convective terms, rather than the original Adams–Bashforth. The computational domain is illustrated in figure 1. Dealiased Fourier expansions are used in the streamwise (x) and spanwise (z) directions, and Chebychev polynomials are used in the wall-normal (y) direction. Boundary conditions are periodic in x and z, and the

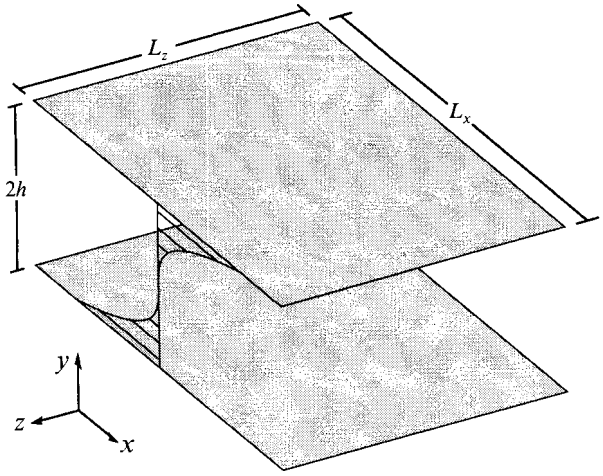

FIGURE 1. Flow geometry. Streamwise and spanwise boundaries are periodic. Top and bottom walls move in the x-direction at velocities U_w and $-U_w$, respectively.

no-slip condition is imposed at the walls. The mean streamwise pressure gradient is zero, and the flow is driven by the motion of the walls.

The flow velocities in the x-, y-, and z-directions are u, v, and w, respectively. The Fourier transforms of the velocities are 'hatted', and are functions of the streamwise wavenumber, k_x, the spanwise wavenumber, k_z, and the untransformed y-coordinate, e.g. $\hat{u}(k_x, y, k_z)$. The 'mean' velocity $\hat{u}(0, y, 0)$, the instantaneous streamwise velocity averaged in the x- and z-directions, is denoted by $U(y)$. The fundamental streamwise and spanwise wavenumbers are $\alpha \equiv 2\pi/L_x$ and $\beta \equiv 2\pi/L_z$, where L_x and L_z denote the streamwise and spanwise dimensions of the computational domain. Quantities have been non-dimensionalized by 'outer' variables: half the wall separation, h, and the wall velocity, U_w. In cases where the 'inner', or 'wall', variables ν and u_τ are used for non-dimensionalization, a $^+$ superscript is used. The flow Reynolds number is given by $Re = U_w h/\nu$.

A computational grid of $16 \times 33 \times 16$ in x, y and z was used for the calculations presented here. Because of the small computational domain, u_τ varies with time, but the resolution in wall units, for the bulk of this study, lies in the range $\Delta x^+ = 10.8$–13.0, $\Delta z^+ = 7.4$–8.9, and $\Delta y^+ = 0.15$–0.18 near the wall, and 3.1–3.7 at the centre of the channel. This resolution is similar to that obtained by Kim, *et al.* (1987).

3. Regeneration cycle

The first step in the study of the regenerative cycle of near-wall turbulent structures was to determine the minimum Reynolds number and minimum dimensions of the periodic domain of a plane Couette flow. Computations for Reynolds number minimization began with random initial conditions at $Re = 625$, a value known to produce sustained turbulence. The resulting flow was allowed to develop in time, the Reynolds number reduced, and the flow once again allowed to evolve. The Reynolds number was reduced in this manner to $Re = 500$ and 400, with turbulence no longer sustained at $Re = 300$. The lateral dimensions of the domain were minimized in a similar fashion, with reductions first in the spanwise dimension, L_z, then in the streamwise dimension, L_x. The final parameter values (except where otherwise noted)

are $L_x = 1.75\pi$ and $L_z = 1.2\pi$ ($L_z^+ = 116.9$–143.6) at $Re = 400$. These values were chosen because they produce a flow which is best suited to the present study, as will be discussed below.

The flow realized in this small domain is ideal for examining the turbulence regeneration mechanisms. Much of the randomness in the location of the turbulence structures is eliminated, and regeneration occurs temporally in a well-defined, quasi-cyclic process. The general characteristics of the flow over one complete regeneration cycle can be seen in figure 2. This is a plot of streamwise (u) velocities in the (x,z)-plane midway between the walls at various times. At the upper left, the flow can be seen to have little x-dependence, and strong streak-like structures dominate the flow. As time increases, the x-dependence increases, with the streaks becoming 'wavy' and then breaking down. By 'breakdown' we mean the production of smaller-scale features and loss of definition of the streak, not the breakdown of Swearingen & Blackwelder (1987), a violent process of scale and structure change during transition to turbulent flow. Finally, in figure 2(h), a well-defined, nearly x-independent streak has been regenerated, and the cycle is ready to repeat.

Because periodic solutions in x and z are used in these simulations, Fourier decomposition is a natural means to study the regeneration cycle. The modal RMS velocity (the square root of the 'kinetic energy') is given by

$$M(k_x = m\alpha, k_z = n\beta) \equiv \left\{ \int_{-1}^{1} \left[\hat{u}^2(m\alpha, y, n\beta) + \hat{v}^2(m\alpha, y, n\beta) + \hat{w}^2(m\alpha, y, n\beta) \right] \mathrm{d}y \right\}^{1/2}, \tag{3.1}$$

and figure 3(a) is a plot of this quantity in various modes over many cycles. The cyclic nature of the flow is particularly apparent in the $(0,\beta)$ and $(\alpha,0)$ modes of this plot. Though $M(0,\beta)$ is summed over all three modal velocity components, the dominant contribution is from $\hat{u}(0,y,\beta)$, the fundamental-in-z, x-independent streamwise velocity mode, i.e. the streaks. The streamwise velocity contours of figure 2 come from a single cycle of the flow of figure 3(a), and the corresponding times are marked, with an expanded scale, in figure 3(b). Note the decrease and then increase in $M(0,\beta)$ as the flow passes from small x-dependence to large x-dependence, and back again.

The period of the regeneration cycle is slightly less than $100\ h/U_w$ ($\approx 270\ \nu/u_\tau^2$), based on 16 cycles in 1500 time units in figure 3. This is approximately the same as the period observed by Jiménez & Moin (1991) in their minimal channel flow at higher Reynolds number, though their channel flow and the present plane Couette flow have slightly different time normalizations. The regeneration cycle can be divided roughly into two phases, each with a duration of about 50 time units: streak formation, where $\mathrm{d}M(0,\beta)/\mathrm{d}t > 0$, and streak breakdown, where $\mathrm{d}M(0,\beta)/\mathrm{d}t < 0$. These are the subjects of the next two sections.

4. Streak formation

Near-wall streaks, elongated regions of spanwise alternating low- and high-speed fluid, can easily be produced by streamwise vortices. Streaks produced in this way are formed in regions where the vortex has a component of velocity across the gradient of streamwise velocity. On one side of the vortex, low-speed fluid is lifted away from the wall by the vortex into a region of higher-speed fluid, producing a low-speed streak, while on the other side of the vortex, high-speed fluid is pushed toward the wall, creating a high-speed streak. This mechanism has been widely discussed by

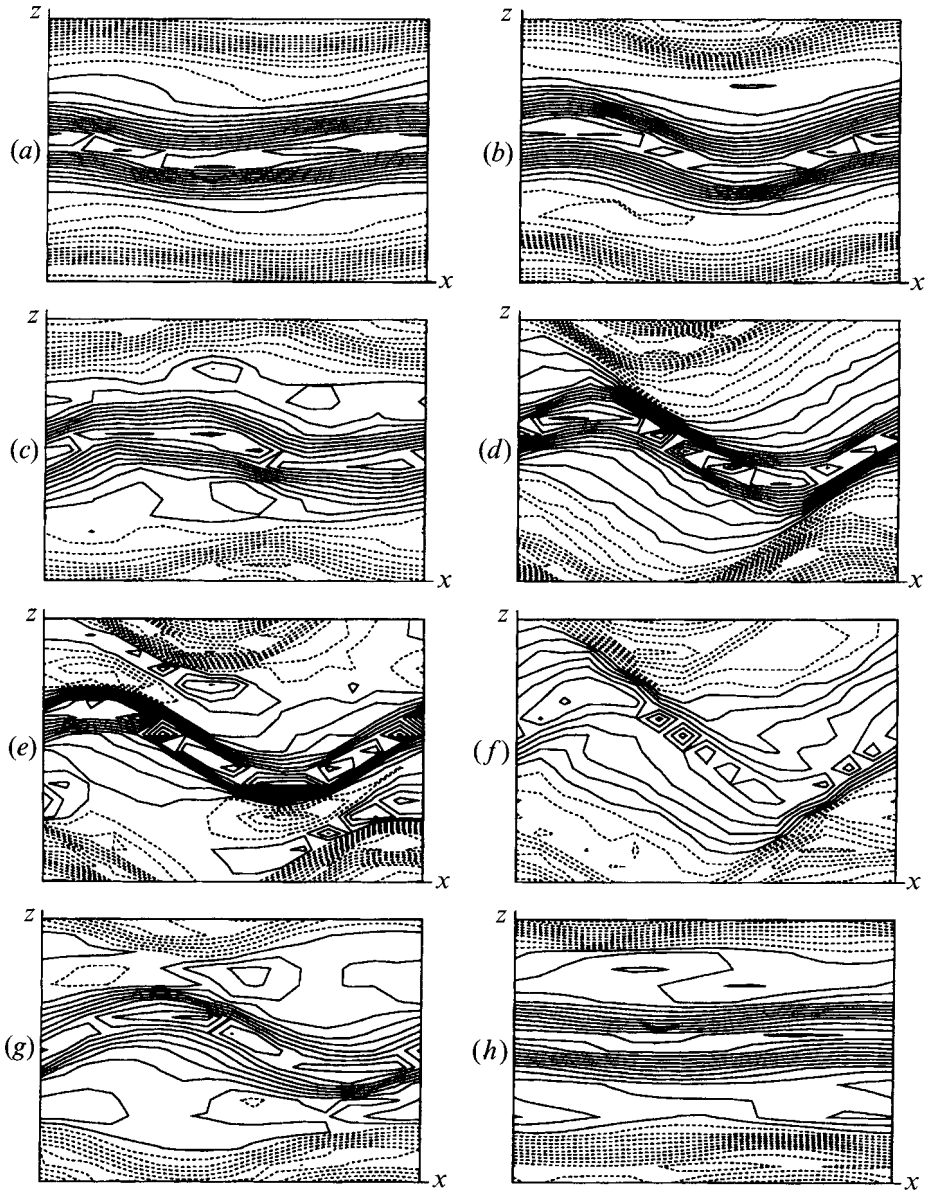

FIGURE 2. Iso-contours of u-velocity in the (x,z)-plane centred between the walls; solid contours positive, dashed contours negative. Contour interval 0.032. (*a*) $t = 757.5$, (*b*) $t = 764.8$, (*c*) $t = 772.0$, (*d*) $t = 777.8$, (*e*) $t = 783.0$, (*f*) $t = 794.1$, (*g*) $t = 808.2$, (*h*) $t = 830.2$.

previous investigators, including Klebanoff, Tidstrom & Sargent (1962), Kline *et al.* (1967), Bakewell & Lumley (1967), and Aubry *et al.* (1988). Mathematically, streak formation by streamwise vortices can be represented as the modification of some suitably averaged mean flow, $\overline{U}(y)$, by advection (e.g. Ellingsen & Palm 1975):

$$-v\frac{\partial \overline{U}(y)}{\partial y} \tag{4.1}$$

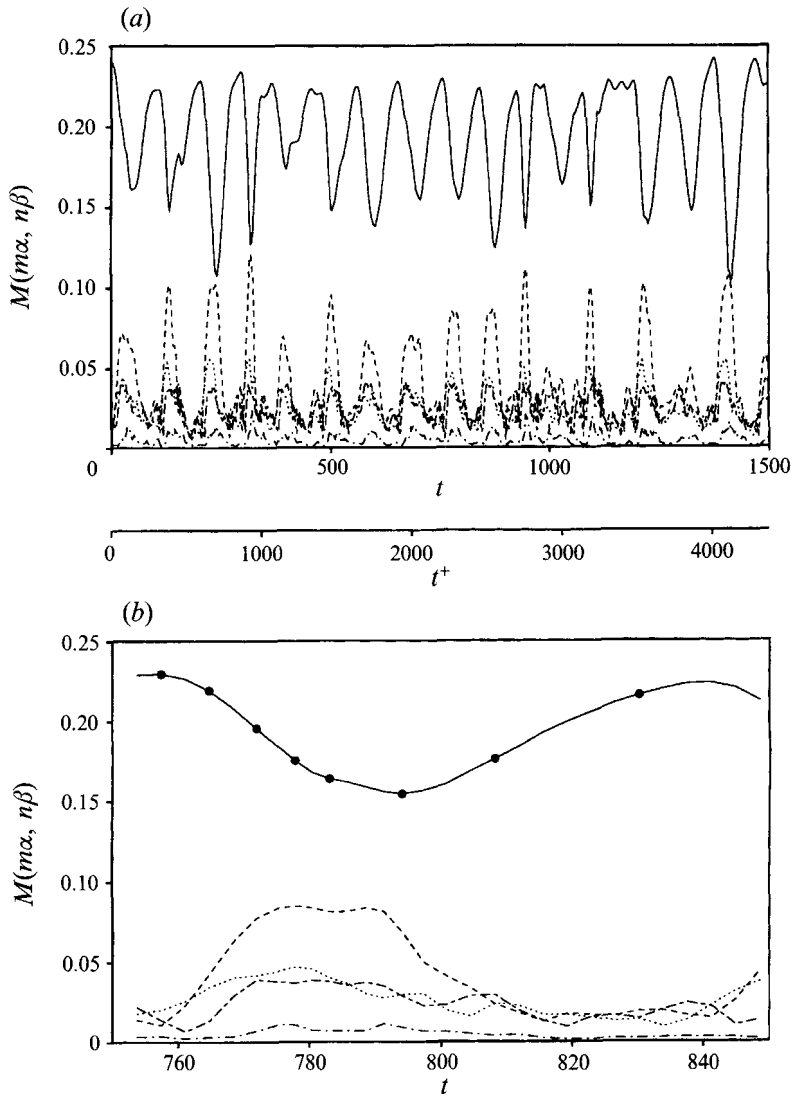

FIGURE 3. Modal decomposition: (*a*) multiple regeneration cycles, (*b*) single cycle of the same flow. ——— , $M(0,\beta)$; - - - - - - - - , $M(\alpha,0)$; ····· $M(\alpha,\beta)$; - - - - - - - , $M(\alpha,2\beta)$; - · - · - · - , $M(2\alpha,0)$. Solid circles on the $M(0,\beta)$ curve in (*b*) are at times which correspond to figure 2(*a–h*).

(note that this is a linear process). In the minimized plane Couette flow of the present study, the streaks occupy the $k_x = 0$ (x-independent) Fourier modes. The dynamics of streak formation, in Fourier space, are thus governed by the various terms in the equation for $\partial\hat{u}(0,y,n\beta)/\partial t$. The linear advection mechanism is represented by

$$-\hat{v}(0,y,n\beta)\frac{\partial U(y)}{\partial y} \tag{4.2}$$

(the Fourier space equivalent of (4.1)). This is the only mechanism by which energy can be transferred directly to the streaks from the mean flow, $U(y)$; there are other $k_x = 0$ interactions, but only the terms of (4.2) can account for extraction of energy

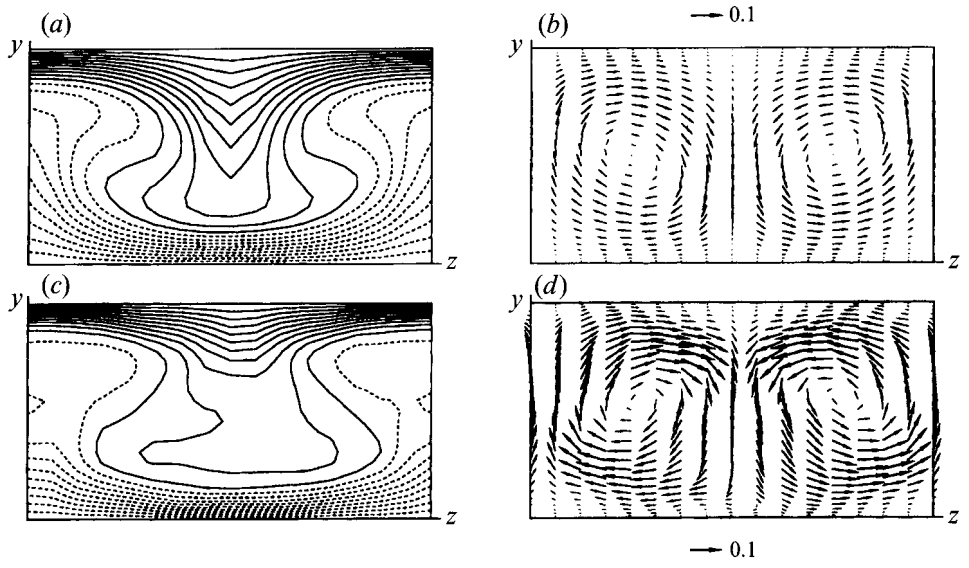

FIGURE 4. Streamwise and cross-flow velocities in the (y,z)-plane for the x-independent modes: (a,b), $t = 757.5$; (c,d), $t = 794.1$. Iso-contours of u in (a) and (c), solid lines are positive values, dashed lines are negative values, contour interval 0.1. The velocity vectors for v, w in (b) and (d) have the same scale. Reference vectors of magnitude 0.1 are plotted.

from $U(y)$. The $k_x = \alpha, 2\alpha, \ldots$ modes can also affect $\hat{u}(0,y,n\beta)$, but not through direct interaction with the mean shear.

Examples of the streaks and streamwise vortices in the present study are plotted in figure 4. Isolines of u, the streaks, and velocity vectors of v and w, the vortices, are plotted in the cross-flow (y,z) plane for the x-independent modes at times corresponding to a maximum and a minimum in $M(0,\beta)$ in figure 3. (Note that the streamwise vortices are stronger after breakdown; this is discussed in §6.) The spatial arrangement of the streaks and vortices is consistent with the notion that the vortices have created the streaks through the linear advection mechanism, but the actual generation of the streaks can be tested. To do this, we examine the results of a series of simulations in which the initial conditions are taken from the regeneration cycle, but with some of the Fourier modes modified.

To examine the formation of streaks by x-independent vortices acting on the mean flow, it is desirable to simulate a flow in which only the vortices are present initially, and to look for the subsequent development of streaks. This is possible when considering the x-independent modes because the cross-flow velocities v and w decouple from the streamwise velocity u: for $u(y,z)$, $v(y,z)$ and $w(y,z)$

$$\frac{\partial v}{\partial t} + v\frac{\partial v}{\partial y} + w\frac{\partial v}{\partial z} = -\frac{\partial p}{\partial y} + \frac{1}{Re}\left(\frac{\partial^2 v}{\partial y^2} + \frac{\partial^2 v}{\partial z^2}\right), \tag{4.3a}$$

$$\frac{\partial w}{\partial t} + v\frac{\partial w}{\partial y} + w\frac{\partial w}{\partial z} = -\frac{\partial p}{\partial z} + \frac{1}{Re}\left(\frac{\partial^2 w}{\partial y^2} + \frac{\partial^2 w}{\partial z^2}\right), \tag{4.3b}$$

$$\frac{\partial v}{\partial y} + \frac{\partial w}{\partial z} = 0. \tag{4.3c}$$

The streaks can be removed numerically by zeroing the $\hat{u}(0,y,n\beta)$ modes for $n \neq 0$,

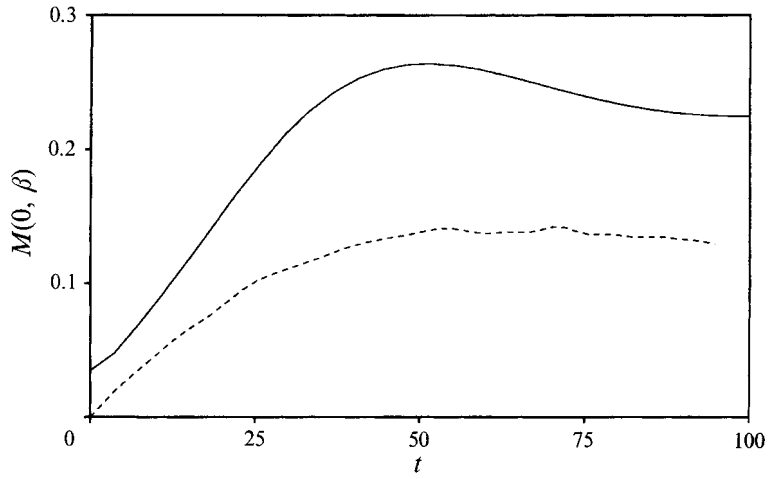

FIGURE 5. Streak formation, growth of the $(0,\beta)$ mode: ——— , growth due to streamwise vortices in $k_x = 0$ modes, initial data $U(y)$ and $\hat{v}$, $\hat{w}(0,y,n\beta)$ at $t = 757.5$ corresponding to a peak in $M(0,\beta)$; ····· , growth due to $k_x = \alpha$ modes, initial data $U(y)$, $\hat{u}$, $\hat{v}$, $\hat{w}(\alpha,y,n\beta)$ at $t = 777.8$ corresponding to a peak in $M(\alpha,\beta)$.

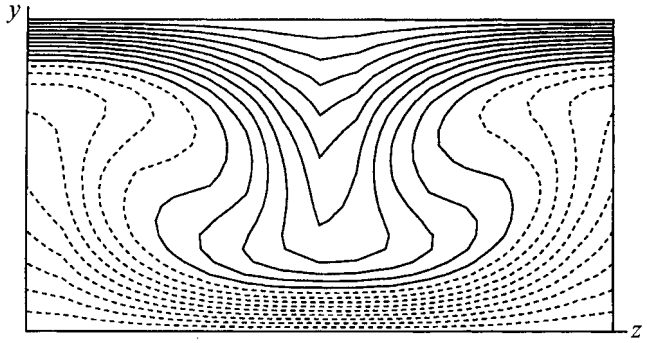

FIGURE 6. Iso-contours of streamwise velocity in the (y,z)-plane at $t = 51.6$ in the simulation of figure 5. Negative contours dashed, contour interval 0.1.

i.e. zeroing all the streamwise velocity Fourier modes in z except the mean (the $k_x \neq 0$ modes of $\hat{u}$, $\hat{v}$, and $\hat{w}$ have already been removed). This has no effect on the vortices because of the decoupling of the velocity components. The initial conditions for the vortices are the same as figure 4(*b*). The cross-flow is held fixed ('frozen') during the computation to prevent decay of the vortices. The resulting growth of the streaks is plotted with a solid line in figure 5, a plot of the growth in $M(0,\beta)$. Note that the time scale of streak generation in this simulation, about 50 time units, is the same as in the full simulation of the regeneration cycle (figure 3). In addition, the streaks formed by the streamwise vortices, in figure 6, are remarkably similar to the streaks of the full simulation in figure 4(*a*).

The formation of streaks by the $k_x = \alpha$ modes was also examined (the reason for investigating the formation of streaks by α-modes will become apparent in §8). The mean velocity profile, $U(y)$, was retained, along with $\hat{u}$, $\hat{v}$, $\hat{w}(\pm\alpha,y,n\beta)$, and all

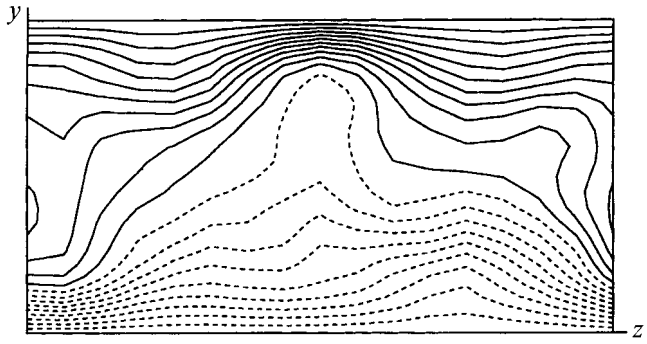

FIGURE 7. Iso-contours of the $k_x = 0$ modes of streamwise velocity generated by interactions of the $k_x = \alpha$ modes. Negative contours dashed, contour interval 0.1.

other modes were zeroed. The α-modes were frozen, and $\hat{v}$, $\hat{w}(0, y, n\beta)$ were fixed at zero. The growth in $M(0, \beta)$ due to these interactions is plotted with a dashed line in figure 5. The time scale is about the same as the $k_x = 0$ interactions, but the amplitude is smaller. More importantly, the resulting 'streaks', plotted in figure 7, are very different from those found in the full simulation. The shapes of the mean flow distortions are different, and have opposite spanwise phase; that is, u is increased where there should be a low-speed streak, and decreased where there should be a high-speed streak.

The mean velocity profile in a laminar plane Couette flow is linear. In a corresponding turbulent Couette flow, turbulent mixing causes higher velocity gradients near the walls, and lower gradients toward the centre of the flow. While the velocity gradient at the wall in the present flow shows moderate variation over the regeneration cycle ($Re_\tau = u_\tau h/\nu = 31.5$–$37.7$), the general shape of the mean velocity profile varies relatively little, as do the shapes of the streamwise vortices (see figure 4*b*, *d*). This suggests that the redistribution of momentum by the vortices may be the primary effect governing the mean velocity profile. To determine whether this is true, the calculations of figures 5 and 6 were repeated with an initially linear 'mean' velocity, $U(y)$ (recall that this 'mean' is the average in the x- and z-directions). The mean velocity profile that develops from these initial conditions is plotted in figure 8 along with the mean profile from the full simulation of the regeneration cycle. The mean profile due to the vortices only is plotted at a time corresponding to a peak in $M(0, \beta)$, similar to the peak in figure 5. The mean profile from the full simulation is at $t = 757.5$. The two profiles are very similar, indicating that the mean profile is, indeed, governed by the streamwise vortices.

5. Streak breakdown

The high- and low-speed streaks in figure 2 are nearly straight initially, with little x-dependence, but they quickly develop a 'waviness' in x and then break down. This can also be seen in the modal energy plot of figure 3(*a*). The peaks in $M(0, \beta)$ correspond to the times at which the streaks have the least x-dependence. As the streaks become wavy $M(0, \beta)$ decreases. Finally, breakdown occurs and $M(0, \beta)$ reaches a minimum. The decrease in $M(0, \beta)$ during streak breakdown is accompanied by a sharp increase

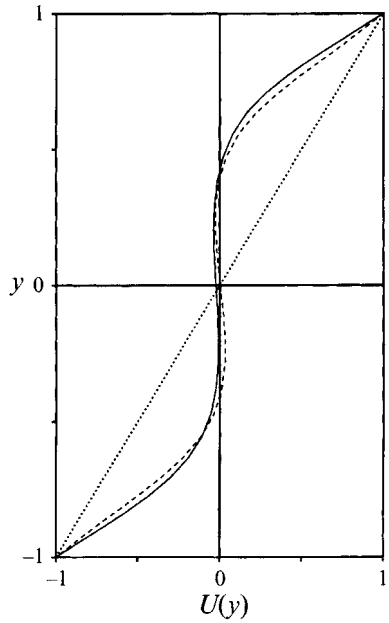

FIGURE 8. Profile of $U(y)$, streamwise velocity averaged in x and z: ——— , profile from full simulation at $t = 757.5$; - - - - - - - - , profile at peak of $M(0,\beta)$ from simulation with initially linear (·····) streamwise velocity profile and streamwise vortices from full simulation at $t = 757.5$.

in energy in the $(\alpha, 0)$ mode, the fundamental-in-x mode with no variation (i.e. no streakiness) in z.

Swearingen & Blackwelder (1987) used Görtler vortices formed in flow along a concave wall to model the near-wall region, and concluded that breakdown was the result of the inflectional instability of the streaks produced by the vortices. In order to determine whether an instability causes breakdown in the present case, the growth or decay of small-amplitude, spatially random fluctuations in an otherwise x-independent flow was examined. The initial conditions consisted of a base flow and small random perturbations. The base flow was obtained from the simulation of figures 2 and 3, at time $t = 757.5$, corresponding to a peak in $M(0,\beta)$. Only the $k_x = 0$ modes of $\hat{u}$, $\hat{v}$ and $\hat{w}$ (i.e. the x-independent modes) were retained. All remaining Fourier modes were replaced with random perturbations, uniformly distributed from zero to $10^{-6}U_w$. The base flow was 'frozen', and the perturbations allowed to evolve normally. This procedure is much like that used to observe the development of streaks in the previous section, except that here both the cross-flow and the streaks are frozen, and it is the growth of perturbations in the x-dependent modes that is of interest. The small initial perturbation amplitudes were chosen in order to study the linear stability of the flow. In effect, this is an indirect way to obtain solutions of the linear eigenvalue problem.

If the base flow is unstable, the fastest growing instability mode would be expected to dominate after sufficient time. In general, this instability mode will consist of many Fourier modes. During the computation, when the amplitude of any Fourier mode grew above some preset threshold, the amplitudes of all perturbations were renormalized to ensure calculation of linear stability. The results of this simulation show that the streaks are indeed linearly unstable. The growth of the most unstable

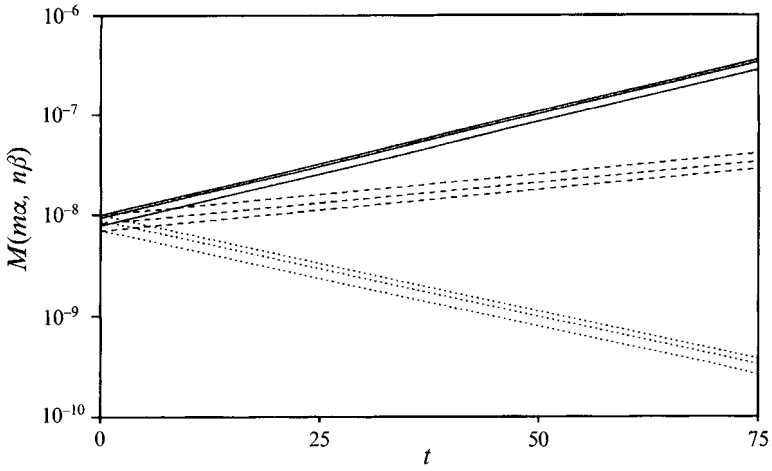

FIGURE 9. Linear stability of $k_x = 0$ modes of flow from full simulation at $t = 757.5$: ———, $(\alpha, 0)$, (α, β) and $(\alpha, 2\beta)$ modes; - - - - - - - -, $(2\alpha, 0)$, $(2\alpha, \beta)$ and $(2\alpha, 2\beta)$ modes; ·····, $(3\alpha, 0)$, $(3\alpha, \beta)$ and $(3\alpha, 2\beta)$ modes.

modes is shown in figure 9. For purposes of this plot, the α, 2α and 3α instability modes obtained from the simulation were normalized to have approximately the same initial amplitude. Note that because the base flow is periodic in z the perturbations must have the form

$$e^{i\alpha x} \sum_n c_n e^{in\beta z}.$$

Thus, the various spanwise Fourier modes that contribute to each instability mode grow at the same (exponential) rate.

Comparison of the linear stability results to the full simulation shows some differences, but these are to be expected, since breakdown is clearly a nonlinear (i.e. finite amplitude) process. The waviness that develops during actual breakdown is not really a 'mode'; for instance, $M(\alpha, 0)$, $M(\alpha, \beta)$ and $M(\alpha, 2\beta)$ do not grow together as a single instability mode in figure 3 as they do in figure 9. In addition, the time scale of the linear instability is too long, with $M(\alpha, 0)$ in figure 3 growing by nearly an order of magnitude in less than 20 h/U_w during breakdown, while the α instability mode in the linear simulation of figure 9 requires nearly 50 time units. The linear approach matches the rapid growth rates of the full simulation only during the initial, transient phase. The principal limitation of the linear approach is that the 'base' flow we are trying to analyse evolves on the same time scale as the instability. The choice of a base flow corresponding to a peak in $M(0, \beta)$ for the stability computation was for this reason somewhat arbitrary. A base flow obtained from data at $t = 753.8$, just slightly before the peak at $t = 757.5$, gives rather different results. At the earlier time, only the α-modes are unstable, while at the later time, both the α- and the 2α-modes grow. Clearly, the linear analysis is sensitive to the details of the base flow. This sensitivity applies also to the shape of the instability modes. In figure 10, the mode shapes, in y, of $\hat{v}(\alpha, y, \beta)$, $\hat{w}(\alpha, y, 0)$ and $\hat{w}(\alpha, y, \beta)$ are plotted. Data from the linear stability computations for $t = 753.8$ and $t = 757.5$ are plotted, along with the actual mode shapes obtained from the simulation at mid-breakdown at $t = 775.1$. Each mode is normalized to give a peak amplitude of 1. The mode shapes calculated from

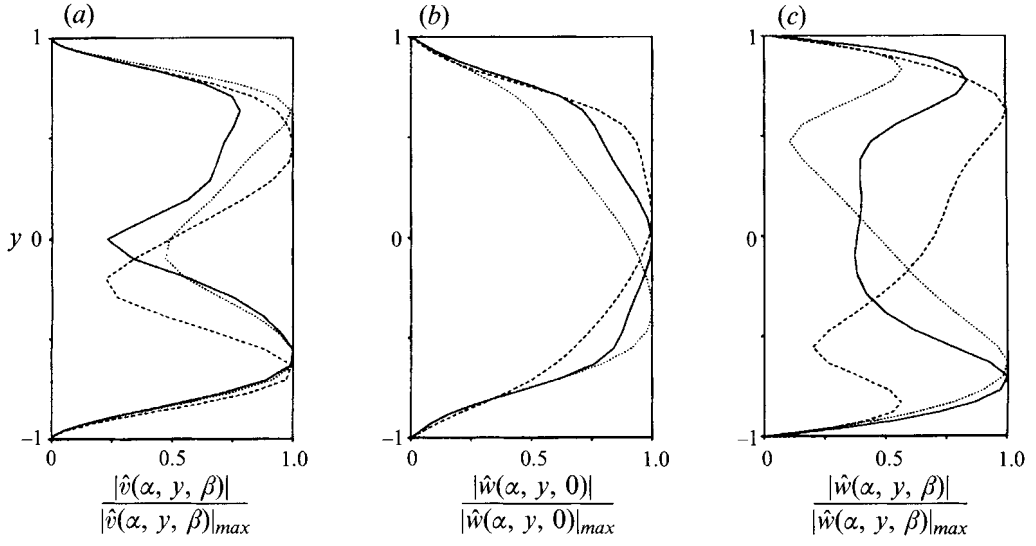

FIGURE 10. Shapes of α-modes due to streak breakdown and linear instability: ———, modes from full simulation at $t = 775.1$; - - - - - - - -, linear stability of $k_x = 0$ modes of full simulation at $t = 753.8$; ·····, linear stability of $k_x = 0$ modes from full simulation at $t = 757.5$. Modes normalized for maximum amplitude of 1. For the full simulation, $|\hat{w}(\alpha, y, 0)|_{max} = 0.16$, $|\hat{v}(\alpha, y, \beta)|_{max} = 0.02$, and $|\hat{w}(\alpha, y, \beta)|_{max} = 0.06$.

the two base flows differ from the actual mode shapes, and they differ as much from each other. But, given that the flow in the full simulation continues to evolve, the mode shapes are surprisingly similar.

The linear approach gives strong evidence that the x-independent base flow is unstable, but the nature of this instability can be explored further with no assumption of linearity by selectively altering various Fourier modes, as was done in §4.

Again, the starting point is the flow of figures 2 and 3 at $t = 757.5$, corresponding to a peak in $M(0, \beta)$. Of the x-dependent Fourier modes, only the fundamental modes, of wavenumber α, are retained; all higher modes (2α, 3α, *etc.*) are set to zero. The amplitudes of the α modes are unaltered. Of the x-independent ($k_x = 0$) Fourier modes, three cases are considered: (i) only $U(y)$, the mean streamwise velocity, is retained, all other modes and velocities are set to zero; (ii) the $\hat{u}(0, y, n\beta)$ Fourier modes (for $n \neq 0$) are set to zero, eliminating the streaks, but retaining the mean streamwise velocity and the streamwise vortices; and (iii) the $\hat{v}(0, y, n\beta)$ and $\hat{w}(0, y, n\beta)$ Fourier modes, for all n, are set to zero, eliminating the streamwise vortices but retaining the streaks and the mean streamwise velocity. Of these three cases, only the last produces growth of the α modes. Clearly, then, it is the instability of the streaks which causes breakdown, not the instability of the mean flow, $\hat{u}(0, y, 0)$, or the streamwise vortices, though, as was seen in §4, it is the streamwise vortices acting on the mean flow which produces the streaks.

6. Streamwise vortex regeneration

The regeneration of turbulence structures, as discussed so far, consists of a continuous cycle of streak formation and breakdown. Streak formation was shown to be the result of momentum redistribution by streamwise vortices (§4). In particular, it

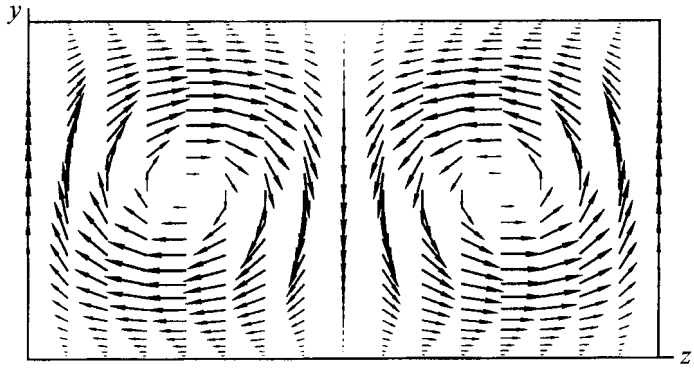

FIGURE 11. Velocity vectors of the most slowly decaying cross-flow eigenmode of x-independent flow. Solution from Waleffe (1991). Mode amplitude is arbitrary.

was shown that the streaky structure in the $\hat{u}(0, y, n\beta)$ modes was due to the $\hat{v}(0, y, n\beta)$ and $\hat{w}(0, y, n\beta)$ modes ($n \neq 0$). This raises the question of how the streamwise vortices are produced.

Some insight into the behaviour of the streamwise vortices can be gained by first examining the characteristics of x-independent flows. Waleffe (1991) has calculated the eigenmodes of the cross-flow (v and w), and the most slowly decaying mode is plotted in figure 11. In this computation, the streamwise flow is irrelevant since v and w decouple from u in x-independent flows, as shown in (4.3). One consequence of this decoupling is that the cross-flow in an x-independent flow must always decay since there is no mechanism by which energy can be transferred from the driven, streamwise flow into the cross-flow. The cross-flow eigenmodes, by definition, have a constant mode shape, or distribution of velocities, and only the magnitude of the velocities can change. The present flow also exhibits a relatively constant velocity distribution in the x-independent modes. In figure 4, it can be seen that the streamwise vortices persist throughout the regeneration cycle with little change in shape, and this shape is quite similar to the most slowly decaying eigenmode of figure 11. However, the streamwise vortices of figure 4 actually become stronger after breakdown, compared to the continuous decay of the eigenmodes. Since it is the α-modes which grow during streak breakdown, it would appear that the strengthening of the vortices is due to interactions among the α-modes. To examine these interactions, we again use simulation data as a starting point.

A close examination of the cycle in question shows that the strength of the streamwise vortices begins to increase at about $t = 772.0$, corresponding to figure 2*c*. The flow field at this time is used as an initial condition, with all modes set to zero except the mean, $U(y)$, and the α-modes: $\hat{u}$, $\hat{v}$, and $\hat{w}$ of $(\alpha, y, n\beta)$ (for all n). In addition, the α-modes are frozen. With this initial condition, streamwise vortices quickly appear, and these vortices then produce streaks, as would be expected (§4). If the α-modes are then 'unfrozen', the flow immediately begins to follow the regenerative cycle normally observed. This process is shown in figure 12. Up to $t = 34.9$, the α-modes are frozen, and $M(0, \beta)$ is seen to rapidly increase. After $t = 34.9$ (the heavy vertical line), the α-modes are unfrozen. The energy in the $(0, \beta)$ mode decreases slightly as breakdown due to the α-modes continues, followed by streak regeneration, and another cycle. This result indicates that it is the nonlinear interactions of the

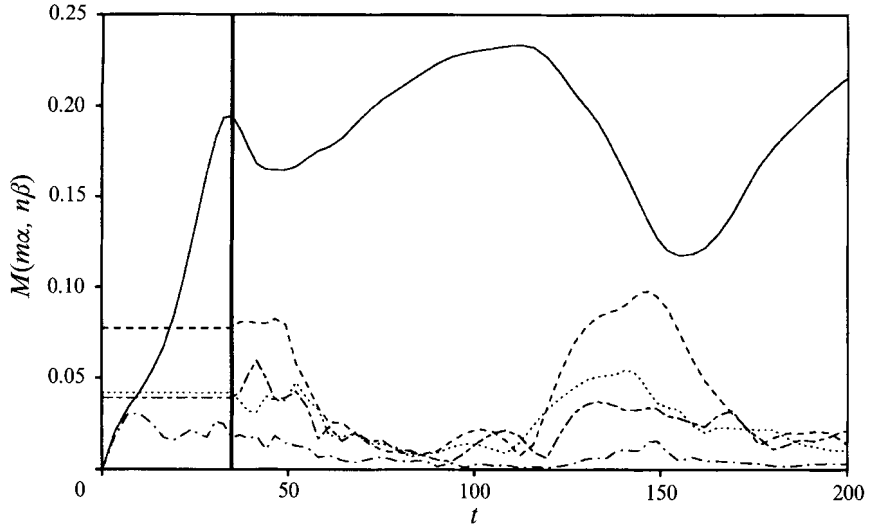

FIGURE 12. Regeneration of streamwise vortices from $k_x = \alpha$ modes, and subsequent reversion to regeneration cycle. Initial conditions: $k_x = \alpha$ modes from full simulation at $t = 772.0$, and all $k_x = 0$ modes zero except $U(y)$. The $k_x = \alpha$ modes are frozen until $t = 34.9$ (heavy vertical line), and thereafter all modes are free to evolve.

α-modes which regenerate the streamwise vortices, but does not reveal the dynamics of the process. The dynamics are most easily studied by an examination of the evolution of streamwise vorticity.

Returning to the full simulation, the cross-flow velocity field and streamwise vorticity field at $t = 772.0$ in the (y, z)-plane are shown in figure 13(a, b). Only the fields due to the $(0, y, \beta)$ modes are shown. Note that each vortex is associated with three distinct regions of vorticity: a large, central region of vorticity of the same sign as the vortex, and two smaller regions, near the walls, of opposite-sign vorticity due to the no-slip wall boundary condition. In Fourier space, the time rate of change of streamwise vorticity, $\partial\hat{\omega}_x(m\alpha, n\beta)/\partial t$, is governed by contributions from six nonlinear terms (neglecting viscosity): the three advection, or redistribution, terms

$$-\hat{u}(p\alpha, q\beta)\frac{\partial\hat{\omega}_x(r\alpha, s\beta)}{\partial x}, \quad -\hat{v}(p\alpha, q\beta)\frac{\partial\hat{\omega}_x(r\alpha, s\beta)}{\partial y}, \quad -\hat{w}(p\alpha, q\beta)\frac{\partial\hat{\omega}_x(r\alpha, s\beta)}{\partial z};$$

and the three 'source' terms

$$\hat{\omega}_x(p\alpha, q\beta)\frac{\partial\hat{u}(r\alpha, s\beta)}{\partial x}, \qquad \hat{\omega}_y(p\alpha, q\beta)\frac{\partial\hat{u}(r\alpha, s\beta)}{\partial y}, \qquad \hat{\omega}_z(p\alpha, q\beta)\frac{\partial\hat{u}(r\alpha, s\beta)}{\partial z}$$

(the y-dependence has been omitted here). The total time rate of change of streamwise vorticity in the $(m\alpha, n\beta)$ mode is the sum of these terms over all values of p, q, r and s such that $p + r = m$ and $q + s = n$. Figure 13(c) is a plot of the contribution of the α-modes to $\partial\hat{\omega}_x(0, \beta)/\partial t$; that is, the sum over all modes for which $p + r = 0$ and $q + s = 1$. A comparison of figures 13(b) and 13(c) shows that, remarkably, the interactions of the α-modes produce additional streamwise vorticity in exactly the right places to augment the streamwise vortices. This alignment of the newly produced streamwise vorticity with the pre-existing vorticity persists throughout the process of vortex regeneration, and is the reason the vortices increase in strength with no significant change in shape, as shown in figure 4(b, d).

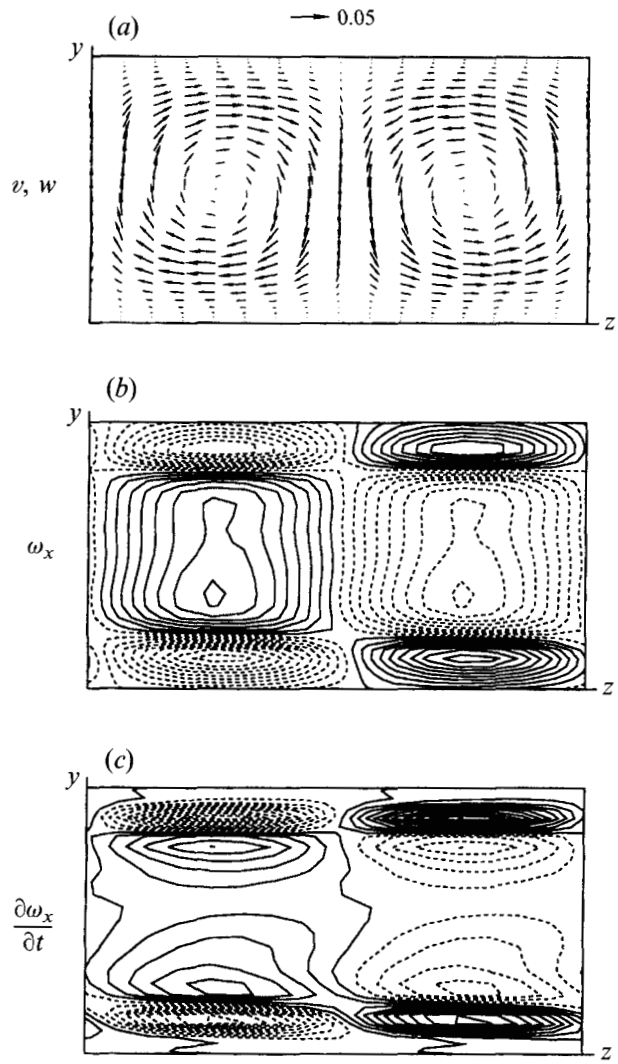

FIGURE 13. Quantities in the cross-flow (y,z) plane at $t = 772.0$ due to the $(0,y,\beta)$ modes only. (*a*) Velocity vectors, reference vector of magnitude 0.05 is plotted; (*b*) streamwise vorticity due to $\hat{\omega}_x(0,y,\beta)$, contour interval 0.015, negative contours dashed; (*c*) time rate of increase in $(0,\beta)$-mode streamwise vorticity due to nonlinear terms only, contour interval 0.005, negative contours dashed.

To compare the contributions of the individual nonlinear terms of the vorticity equation over time it is easiest to consider

$$\frac{\partial|\hat{\omega}_x|^2}{\partial t} = \hat{\omega}_x^\dagger \frac{\partial \hat{\omega}_x}{\partial t} + \hat{\omega}_x \frac{\partial \hat{\omega}_x^\dagger}{\partial t}$$

(where the † superscript indicates the complex conjugate), since this quantity is positive at y-locations where the existing streamwise vorticity is being augmented, and negative where the vorticity is being reduced. The contributions of each term for many wavenumber-pair interactions, integrated in y, are plotted in figure 14(*a*). The sum of the contributions of all the modes is denoted by the heavy solid line

in the figure. The cumulative augmentation of the vortices (i.e. time integration of figure 14*a*) is plotted in figure 14(*b*). Only the α-modes are plotted, since the contributions of interactions of the higher x-wavenumber modes to the $(0,\beta)$ mode are negligible. Note that only the nonlinear terms are being represented in these plots, and the continuous viscous decay of the vortices is not considered. One might hope, for simplicity, that only a single term of the vorticity equation would be dominant. In fact, the plot shows that the largest contribution is from the term

$$-\hat{\omega}_x^\dagger(0,\beta)\left[\hat{v}(\alpha,\beta)\frac{\partial\hat{\omega}_x(-\alpha,0)}{\partial y}+\hat{v}(-\alpha,\beta)\frac{\partial\hat{\omega}_x(\alpha,0)}{\partial y}\right]+\text{c.c.}, \tag{6.1}$$

but this term accounts for only about half of the total vortex augmentation, and the terms

$$\hat{\omega}_x^\dagger(0,\beta)\left[\hat{\omega}_z(\alpha,-2\beta)\frac{\partial\hat{u}(-\alpha,3\beta)}{\partial z}+\hat{\omega}_z(-\alpha,-2\beta)\frac{\partial\hat{u}(\alpha,3\beta)}{\partial z}\right]+\text{c.c.}, \tag{6.2}$$

$$\hat{\omega}_x^\dagger(0,\beta)\left[\hat{\omega}_y(\alpha,3\beta)\frac{\partial\hat{u}(-\alpha,-2\beta)}{\partial y}+\hat{\omega}_y(-\alpha,3\beta)\frac{\partial\hat{u}(\alpha,-2\beta)}{\partial y}\right]+\text{c.c.}, \tag{6.3}$$

$$-\hat{\omega}_x^\dagger(0,\beta)\left[\hat{u}(\alpha,\beta)\frac{\partial\hat{\omega}_x(-\alpha,0)}{\partial x}+\hat{u}(-\alpha,\beta)\frac{\partial\hat{\omega}_x(\alpha,0)}{\partial x}\right]+\text{c.c.}, \tag{6.4}$$

$$\hat{\omega}_x^\dagger(0,\beta)\left[\hat{\omega}_x(\alpha,0)\frac{\partial\hat{u}(-\alpha,\beta)}{\partial x}+\hat{\omega}_x(-\alpha,0)\frac{\partial\hat{u}(\alpha,\beta)}{\partial x}\right]+\text{c.c.} \tag{6.5}$$

are also significant. The c.c. denote the complex conjugates, and the y-dependence has been omitted. Equations (6.4) and (6.5) can be shown to be identical and appear as single lines in figure 14(*a*, *b*). The spatial distributions of the dominant terms of $\partial\omega_x(0,\beta)/\partial t$ at $t = 772.0$ are plotted in figure 15. The contributions of the terms of figures 15(*a*), 15(*b*) and even 15(*c*) have approximately the correct overall spatial distribution to augment the streamwise vortices (i.e. the same distribution as the vorticity in figure 13*b*). The term of figure 15(*d*), however, has a much different spatial distribution, and the vorticity associated with this term tends to reduce the strength of the vortices. The dashed lines in figure 14(*a*, *b*) are due to this interaction, and reflect the negative contribution of this term to $\partial|\hat{\omega}_x|^2/\partial t$. Several pairs of terms, such as (6.2) and (6.3), produce approximately equal and opposite contributions, and would appear to tend to cancel each other. The plots of figure 15(*b*, *d*), however, show that the cancellation is not point by point, but only on average over the height of the channel.

While (6.1)–(6.5) represent modal interactions in Fourier space, each has a physical interpretation, as well. Consider (6.1) near one wall. The $\hat{\omega}_x(\alpha,0)$ modes consist of streamwise alternating sheets of ω_x that are 'anchored' at the wall and incline sharply downstream. The α part (x-dependence) of $\hat{v}(\alpha,\beta)$ tends to force these inclined sheets into alignment with the flow, by pushing, say, positive ω_x away from the wall at one x-location, and pushing positive ω_x toward the wall a distance $L_x/2$ downstream. That portion of ω_x that does align with the flow becomes x-independent. The β part (z-dependence) of $\hat{v}(\alpha,\beta)$ causes this alignment of streamwise vorticity to occur with opposite phase at spanwise separations of $L_z/2$. This is exactly the x-independent, fundamental-in-z rearrangement of vorticity required to produce the elongated streamwise vortices that correspond to the $\hat{\omega}_x(0,\beta)$ mode.

Only a single cycle has been examined in detail here, and it should be noted that there are definite cycle-to-cycle variations. The contribution of (6.1) is almost

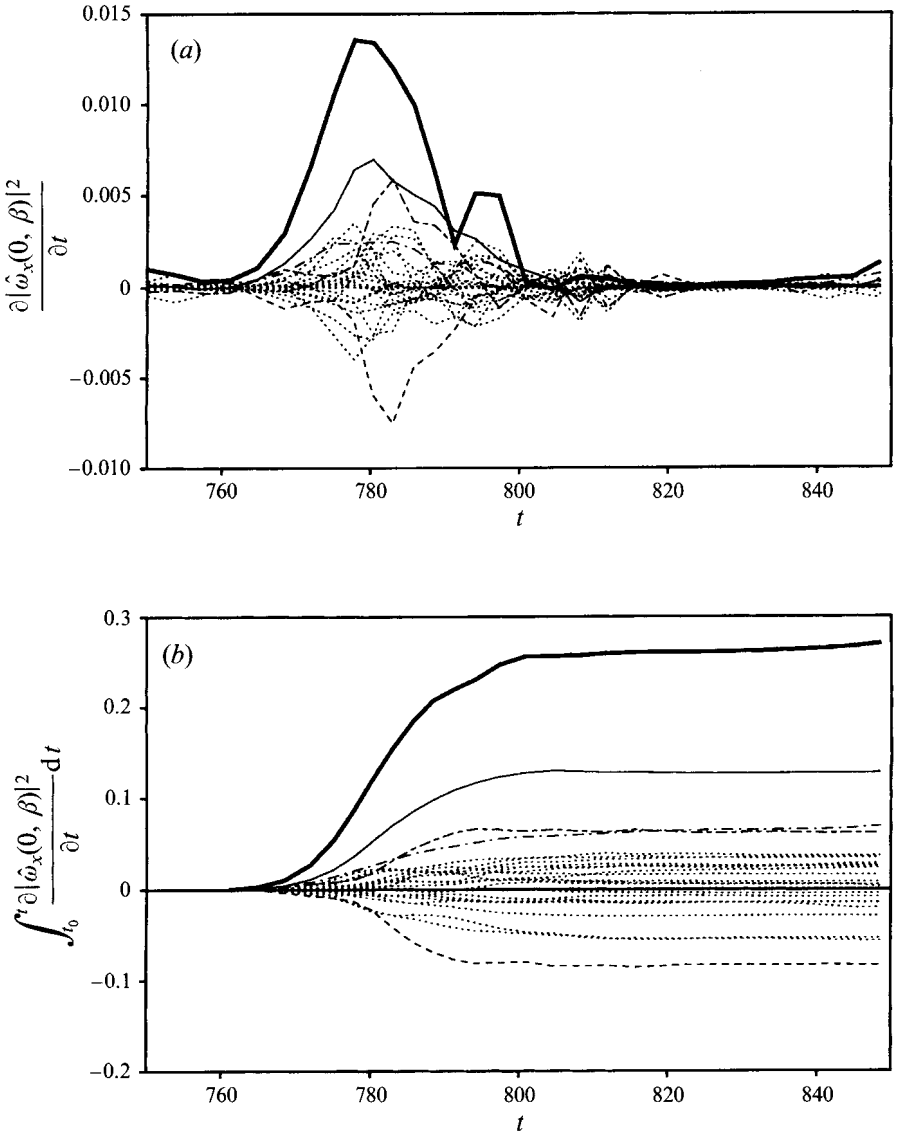

FIGURE 14. Contributions of various terms to (*a*) $\partial|\hat{\omega}_x(0,\beta)|^2/\partial t$, integrated in y, and (*b*) cumulative contribution integrated from $t_0 = 761.1$. ——, summation of all terms, all interactions; — — —, equation (6.1); - - - - - - - -, equation (6.2); – – – – –, equation (6.3); – · – · –, equations (6.4) and (6.5); ·····, all other $(\pm\alpha, 0)$, $(\pm\alpha, \pm\beta)$, $(\pm\alpha, \pm 2\beta)$ and $(\pm\alpha, 3\beta)$ interactions.

always largest, but the other terms vary in their importance. There is also a variation during some cycles in the spatial distribution of vorticity produced during vortex regeneration and, interestingly, vortex regeneration is nearly absent for some cycles. This is evident in figure 16, a plot of $\partial|\hat{\omega}_x(0,\beta)|^2/\partial t$ over many cycles, along with $M(0,\beta)$ for reference. Regeneration is almost negligible, in this figure, for the cycles at $t \approx 1000$ and $t \approx 1300$. If there is no regeneration of the streamwise vortices, how is

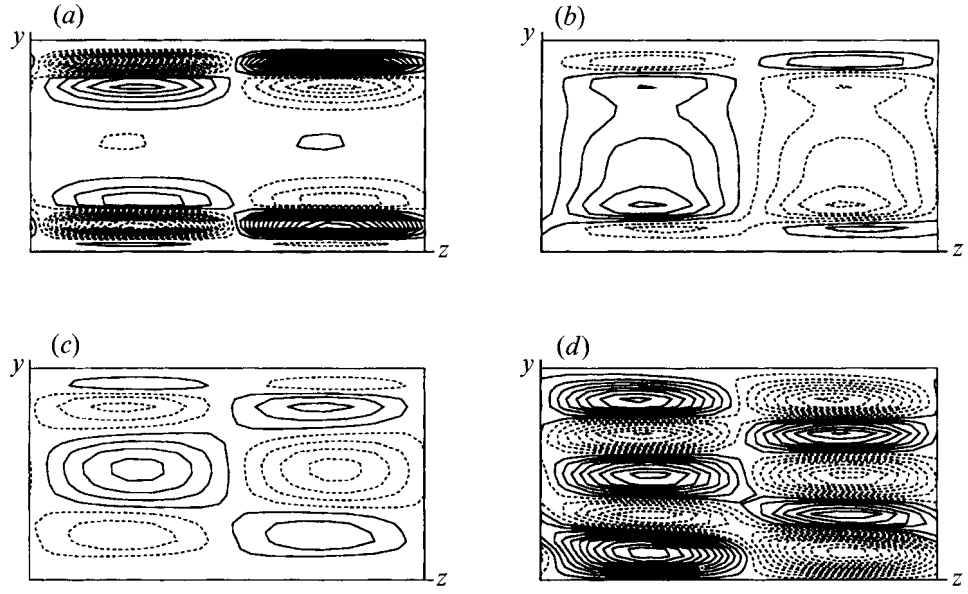

FIGURE 15. Spatial distribution of the most dominant terms of $\partial\hat{\omega}_x(0,\beta)/\partial t$ at $t = 772.0$ (inverse Fourier transform for physical space representation). Solid contours, positive values; dashed contours, negative values. Contour interval 0.002. (*a*) $-\hat{v}(\alpha,\beta)\partial\hat{\omega}_x(-\alpha,0)/\partial y - \hat{v}(-\alpha,\beta)\partial\hat{\omega}_x(\alpha,0)/\partial y$ (cf. equation (6.1)); (*b*) $-\hat{u}(\alpha,\beta)\partial\hat{\omega}_x(-\alpha,0)/\partial x - \hat{u}(-\alpha,\beta)\partial\hat{\omega}_x(\alpha,0)/\partial x$ and $\hat{\omega}_x(\alpha,0)\partial\hat{u}(-\alpha,\beta)\partial x + \hat{\omega}_x(-\alpha,0)\partial\hat{u}(\alpha,\beta)\partial x$ (cf. equations (6.4) and (6.5)); (*c*) $\hat{\omega}_y(\alpha,3\beta)\partial\hat{u}(-\alpha,-2\beta)/\partial y + \hat{\omega}_y(-\alpha,3\beta)\partial\hat{u}(\alpha,-2\beta)/\partial y$ (cf. equation (6.3)); (*d*) $\hat{\omega}_z(\alpha,-2\beta)\partial\hat{u}(-\alpha,3\beta)/\partial z + \hat{\omega}_z(-\alpha,-2\beta)\partial\hat{u}(\alpha,3\beta)/\partial z$ (cf. equation (6.2)).

it possible that the turbulence is sustained? Experiments by Hamilton & Abernathy (1994) showed that, in a laminar flow, streamwise vortices must have a circulation above some threshold in order to cause transition to turbulence. The analogous statement for near-wall streamwise vortices in a turbulent flow would be that the vortices must have a circulation above a threshold in order to produce unstable streaks. If this is the case, regeneration of the vortices need not occur every cycle as long as vortex circulation does not decay below the threshold before subsequent cycles. The circulation of the $k_x = 0$ mode streamwise vortices, $\Gamma_{k_x=0}$, is plotted in figure 17. The circulation peaks during breakdown and then decays. The streaks form as the vortices decay, and the maximum in $M(0,\beta)$ corresponds closely to the minimum in $\Gamma_{k_x=0}$. Therefore, the threshold applies to the minimum values of $\Gamma_{k_x=0}$; the maximum values are relatively unimportant. Hamilton & Abernathy found that the threshold value of the circulation, using the present non-dimensionalization, is about 0.15 in a steady flow. This is consistent with figure 17 since the minimum circulations are never much below that value, even during the two cycles which have no regeneration of the vortices. The circulation of the vortices will also be considered in flows with unsustained turbulence in the next section.

7. Streak spacing

Jiménez & Moin (1991) found that when the spanwise dimension of their computational domain was less than the typically observed spanwise spacing of the streaks, turbulence could not be sustained. As discussed in §1, this led Waleffe *et al.* (1993) to

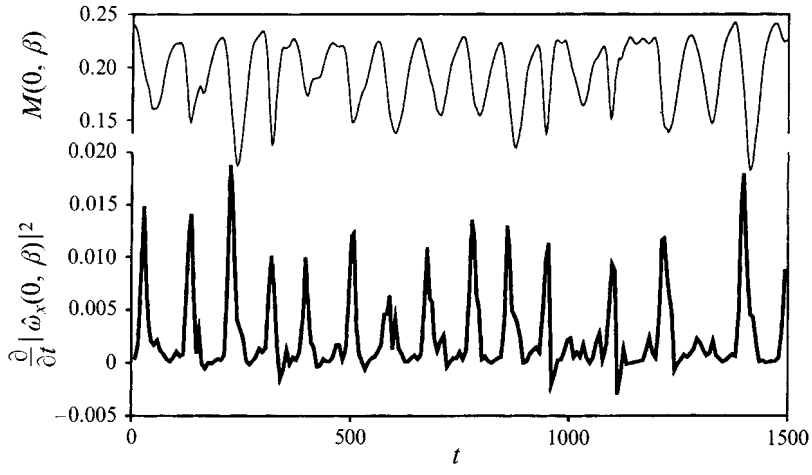

FIGURE 16. Vortex regeneration over multiple cycles.

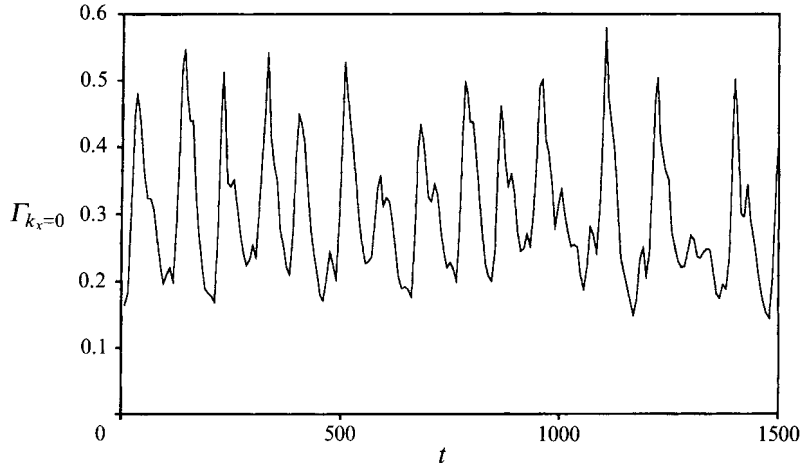

FIGURE 17. Circulation of streamwise vortices in $k_x = 0$ modes. $\Gamma_{k_x=0} \equiv \int \hat{\omega}_x(0, y, n\beta)\mathrm{d}A$. Circulation plotted is based on the contour that gives the maximum circulation from among all rectangular contours on computational grid points in the (y, z)-plane.

conjecture that the streak spacing corresponds to a critical Reynolds number for the entire self-regeneration process. The regeneration process has been examined in some detail in previous sections, and the techniques developed to investigate regeneration can now be used to address the issue of the spanwise spacing of near-wall structures. To do this, we reduce the dimensions of the computational domain in stages, first to a width which, though smaller, will still allow sustained turbulence, and then to a domain so narrow that turbulence is not sustained. We can then establish whether a single step in the regeneration process is disrupted by the constraint of the reduced spanwise dimension, or whether, as Waleffe *et al.* conjectured, the entire process is affected.

The regeneration cycle in a flow with domain dimensions $L_x = 1.58\pi$, $L_z = 1.1\pi$ ($L_z^+ = 103.0$–130.3) and $Re = 400$ is plotted in figure 18. The only notable difference

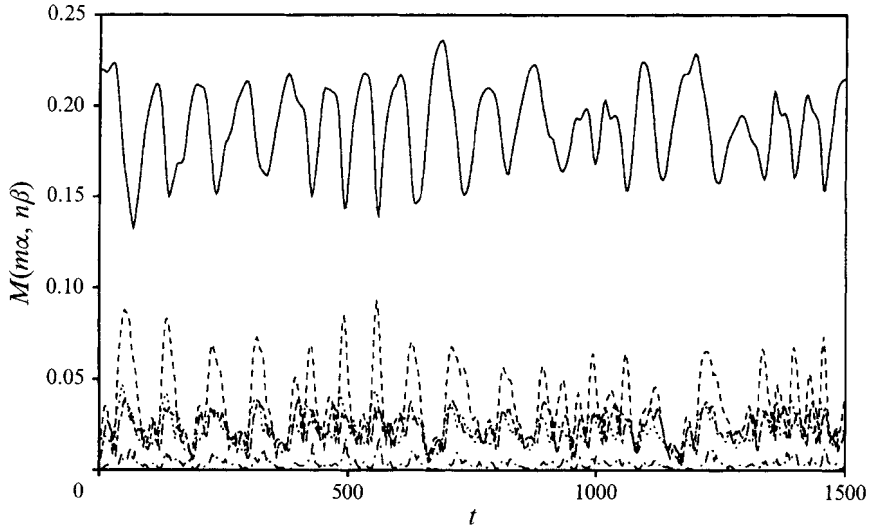

FIGURE 18. Modal decomposition of many regeneration cycles in a reduced domain. Line types correspond to same modes as figure 3(*a*).

between this figure and figure 3(*a*) ($L_z^+ = 116.9$–143.6) is that the 'period' of each cycle is slightly shorter, with 18 cycles in 1500 time units, rather than 16. The streak formation, streak breakdown, and vortex regeneration processes were also compared for the two cases, and some differences were observed. First, there is less likely to be a single dominant term among the contributions to $\partial|\hat{\omega}_x(0,\beta)|^2/\partial t$, though the term of (6.1) is usually slightly larger than any other. Also, the vortex regeneration mechanism tends to produce opposite-signed vorticity at the centre of each vortex, as shown in figure 19 (compare to figure 13). This distribution of $\partial\omega_x/\partial t$ is typical for most vortex regeneration events with this domain size, but exceptions are more frequent than with the larger domain size. None of these effects is particularly significant, since the turbulence is sustained, but they do suggest a subtle shift in the dynamics of the mechanism as L_z^+ decreases.

The dimensions, L_x and L_z, of the computational domains considered up to now were, as mentioned earlier, near the minimum values required to sustain turbulence, but they were not the absolute minimum values. The modal energies in the flow of figure 3 have a well-defined, quasi-cyclic behaviour while some of the other domain dimensions considered, but not presented here, produced flows with much more chaotic cycles. Obviously, streak breakdown is affected by the choice of the streamwise dimension, L_x, since this choice determines α, the streamwise wavenumber of the instability, and the optimum value of α is itself determined by the choice of L_z. Other processes, such as vortex regeneration, may also be affected by the choice of domain dimensions.

When choosing a domain in which the spanwise dimension has been reduced to a value too small to sustain turbulence, these same considerations apply: we wish to find a domain which produces a relatively regular and well-defined regeneration cycle before the turbulence decays. Two such cases of unsustained turbulence are considered here.

The modal decomposition of the first flow is plotted in figure 20. The spanwise dimension of the flow is $L_z = 1.1\pi$, or $L_z^+ = 109.2$ to 126.1 (where L_z^+ is based on u_τ

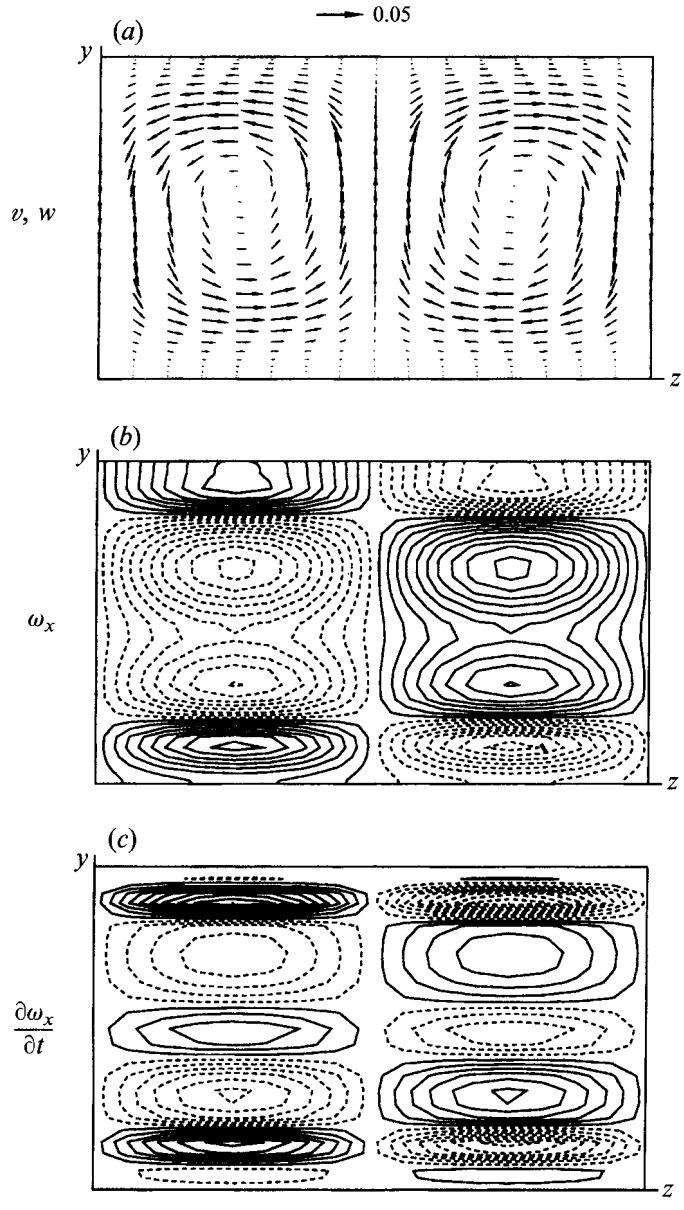

FIGURE 19. Quantities in the cross-flow (y,z) plane at $t = 555.0$ due to the $(0,y,\beta)$ modes only. (*a*) Velocity vectors, reference vector of magnitude 0.05 is plotted; (*b*) streamwise vorticity due to $\hat{\omega}_x(0,y,\beta)$, contour interval 0.015, negative contours dashed; (*c*) time rate of increase in $(0,\beta)$-mode streamwise vorticity due to nonlinear terms only, contour interval 0.004, negative contours dashed.

during the early part of the simulation before the turbulence begins to decay). The streamwise dimension is $L_x = 1.6\pi$, and the same Reynolds number, 400, is used. This flow was obtained by first reducing the spanwise dimension of a sustainable turbulent flow, and then the streamwise dimension.

The quasi-cyclic behaviour of the modal energies in the unsustained turbulent flow of figure 20 appears similar to that of the sustained flow until the final peak in

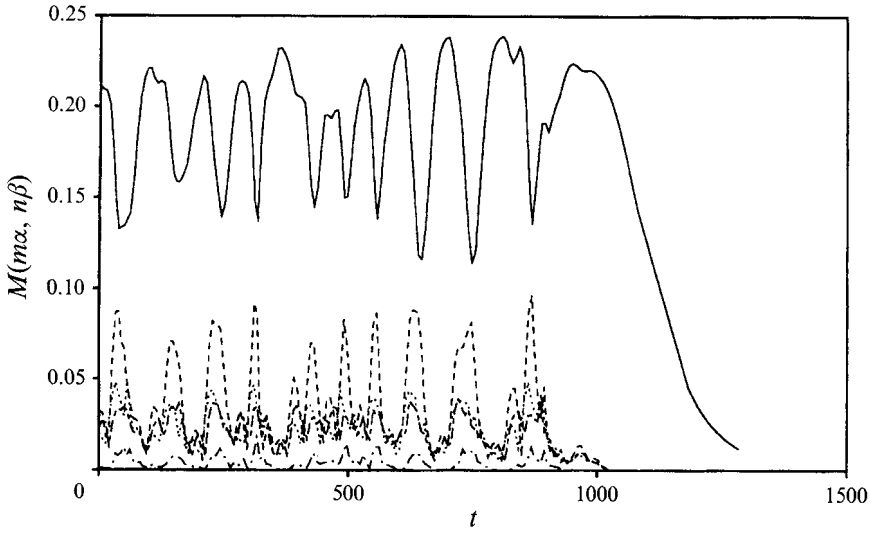

FIGURE 20. Modal RMS velocity over many regeneration cycles of an unsustained turbulent flow. Plotted modes same as figure 3.

$M(0,\beta)$. There is no breakdown of the flow after this peak, and the energies of all the modes decay (except $M(0,0)$, not shown) as the flow becomes laminar. In §5 it was shown that breakdown is the result of an instability of the x-independent ($k_x = 0$) modes of the flow; thus, the absence of breakdown after the final peak would imply that the flow has become stable. To check this, the linear approach of §5 was used to examine the stability of the unsustained turbulent flow at several different times, and the x-independent modes are indeed found to have a dramatic increase in stability for the final, decaying cycle. This result is shown in figure 21 for $t = 603.4$, three cycles before the turbulence decays; at $t = 947.7$, the final peak in $M(0,\beta)$; and a short time later at $t = 981.3$. At the earliest time, the flow is linearly unstable, with a growth rate of the α-modes approximately the same as the sustained flow of figure 9. At $t = 947.7$, the flow is unstable, but with a much lower growth rate. Finally, at the latest time, the flow is linearly stable. Because of this increase in the stability of the flow, breakdown does not occur.

In the sustained turbulent flow, breakdown is the result of the instability of the streaks, and the streaks are the result of advection of momentum by streamwise vortices. Whatever changes occur in the streaks to increase their stability in the unsustained turbulent flow are likely then to be traceable to changes in the streamwise vortices. The regeneration of the streamwise vortices for the last few cycles of the unsustained turbulent flow is shown in figure 22, a plot of $\partial|\hat{\omega}_x(0,\beta)|^2/\partial t$ integrated in y. Also plotted is the RMS of the $(0,\beta)$ mode. Note that the first two vortex regeneration events in the plot peak during streak breakdown, while the final event does not peak until the new streaks have already begun to form. Thus, even though the peak amplitude of the vortex regeneration process is nearly constant for each of the three regeneration events plotted, the final regeneration occurs late relative to the beginning of streak formation. The circulation of the vortices is plotted in figure 23, and it can be seen that the streamwise vortices continue to decay during this delay, with the circulation falling to about 0.11 before regeneration begins. This value is lower than any observed during the sustained cycle of figure 17. After regeneration

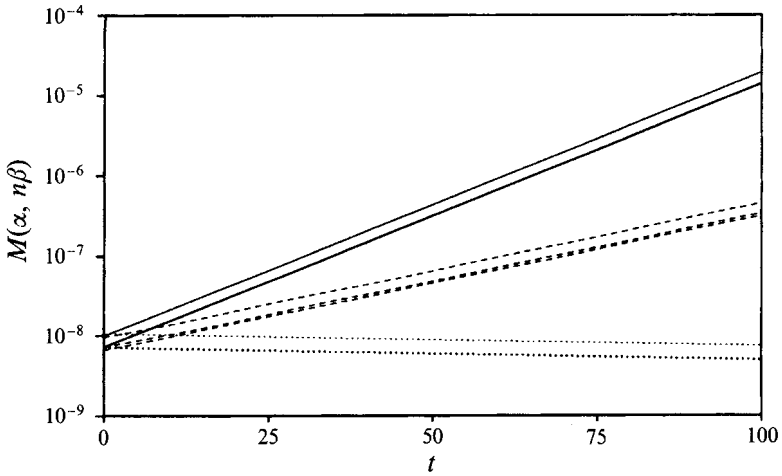

FIGURE 21. Linear stability of unsustained turbulent flow at various times: ——— , $t = 603.4$; - - - - - - - - , $t = 947.7$; ····· , $t = 981.3$. The energies of the $(\alpha, 0)$, (α, β) and $(\alpha, 2\beta)$ instability modes for the flow at each time are shown.

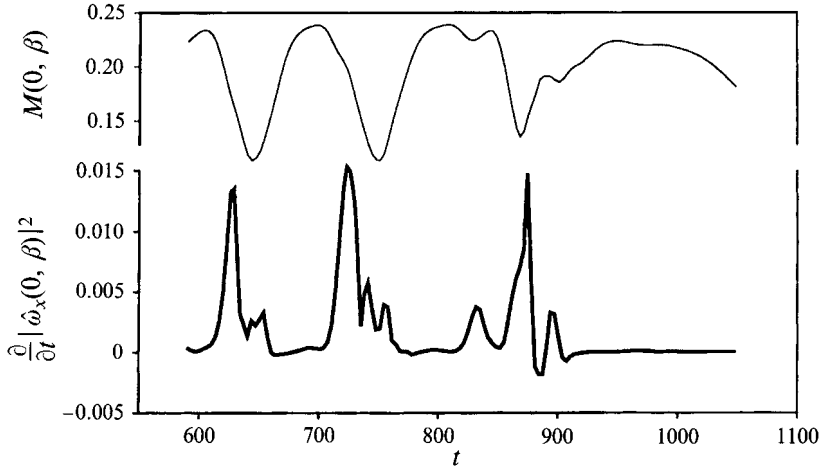

FIGURE 22. Time history of vortex regeneration compared to $M(0, \beta)$: ———, $\partial/\partial t|\hat{\omega}_x(0, \beta)|^2$, integrated in y, contribution of all terms, all interactions; ——— , $M(0, \beta)$.

finally takes place, the circulation drops to about 0.09 at the final maximum in $M(0, \beta)$, and there is no subsequent breakdown.

To verify that the relative delay in vortex regeneration does indeed cause the turbulence to decay, the strength of the streamwise vortices was artificially boosted at $t = 858.5$, a time corresponding to mid-breakdown in the final full regeneration cycle of figure 22. The result is plotted in figure 24. The strength of the vortices was increased by multiplying all the $\hat{v}(0, y, n\beta)$ and $\hat{w}(0, y, n\beta)$ modes by a factor of 2.0, and all other modes were left unmodified. The effect of increasing the vortex strength is immediate and the flow returns to the normal regeneration cycle. Note that the turbulence does not subsequently decay; the domain size is such that turbulence is

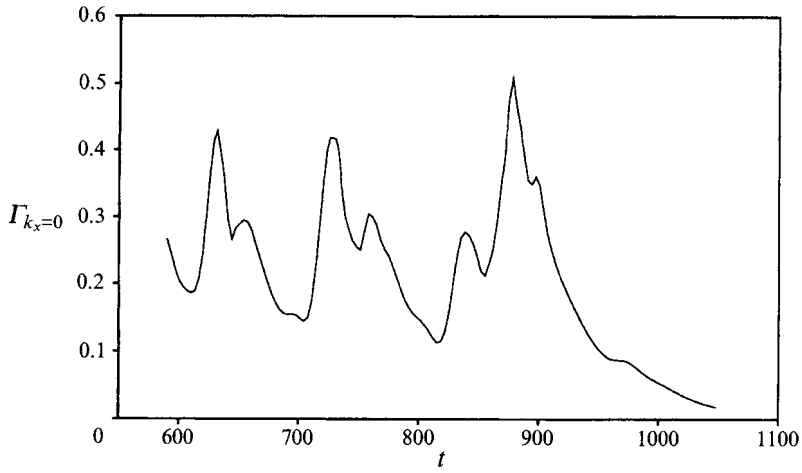

FIGURE 23. Circulation of the streamwise vortices in the $k_x = 0$ modes for the flow of figures 20, 22.

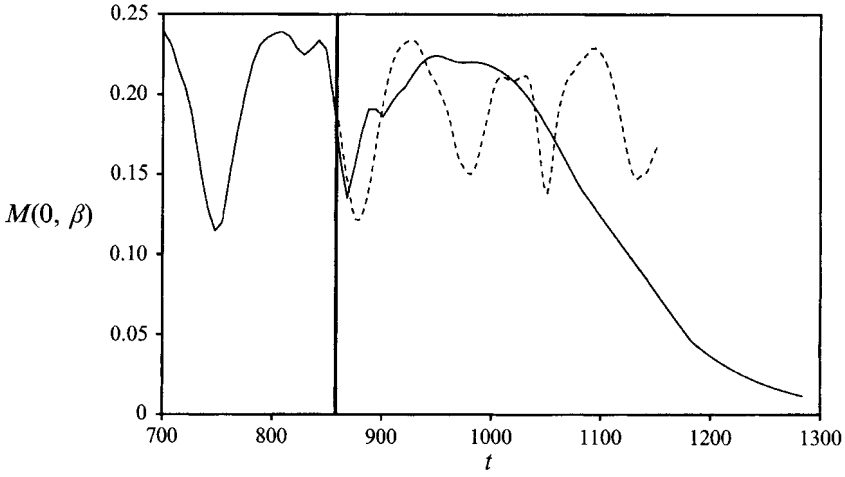

FIGURE 24. $M(0,\beta)$ for: ———, unsustained turbulent flow of figure 20; --------, the same flow with $\hat{v}(0, y, n\beta)$ and $\hat{w}(0, y, n\beta)$ modes multiplied by 2.0 at $t = 858.5$ (denoted by heavy vertical line).

marginally sustainable and can go through a relatively large number of cycles before decaying.

A second case of unsustained turbulence ($L_z^+ = 97.0$–86.5) is presented in figure 25. The solid line in the in the upper half of the plot is $M(0,\beta)$, and the associated vortex regeneration, $\partial|\hat{\omega}_x(0,\beta)|^2/\partial t$, is shown in the lower half. In this flow, vortex regeneration takes place at about the same point in the cycle as in the sustained cases, and the circulation, plotted in figure 26, is increased appropriately. Thus, there is no delay in regeneration as in the previous flow. In this case, the opposite is true, and vortex regeneration takes place too early; at the time of the final peak in $M(0,\beta)$ in figure 25, $\Gamma_{k_x=0}$ has dropped to about 0.1. To verify this assertion, $\Gamma_{k_x=0}$ was increased by a factor of 1.5 at $t = 130.0$ (the peak in circulation in figure 26) and $M(0,\beta)$ of the resulting flow is plotted as a dashed line in figure 25. The increase in circulation produces unstable streaks, followed by breakdown and a return to a (rather chaotic)

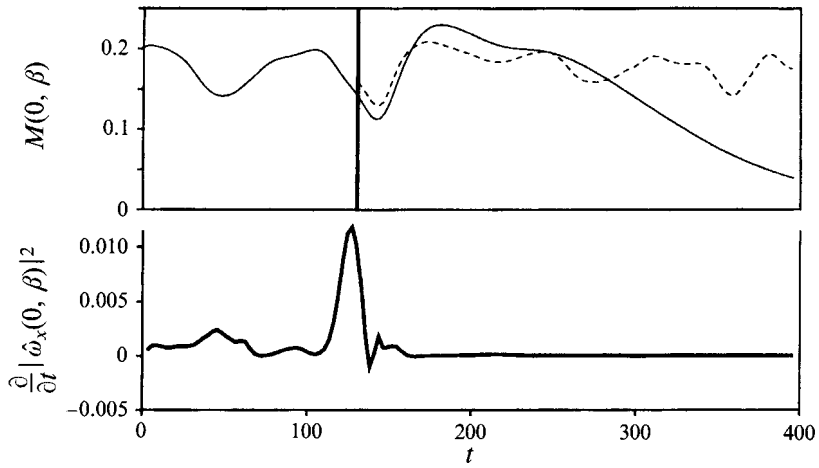

FIGURE 25. $M(0,\beta)$ for flow with $L_x = 1.35\pi$, $L_z = 0.9\pi$ ($L_z^+ =$), and $Re = 400$: ———, unsustained turbulent flow; --------, same flow with $\hat{v}(0, y, n\beta)$ and $\hat{w}(0, y, n\beta)$ modes multiplied by 1.5 at peak in circulation at $t = 130.0$ (denoted by heavy vertical line).

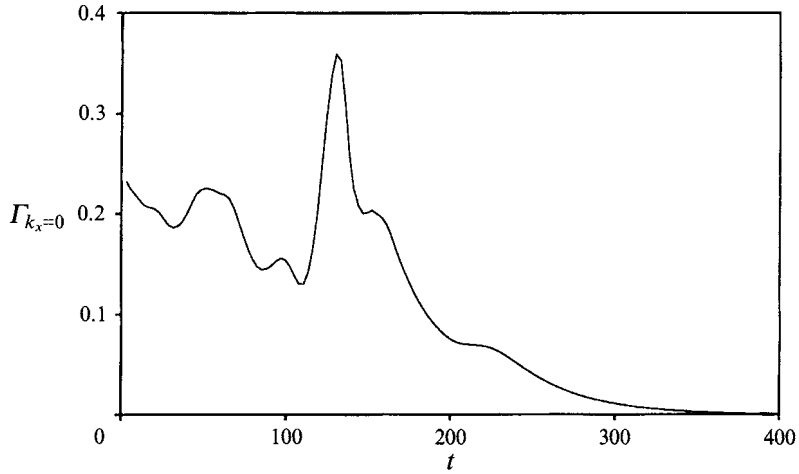

FIGURE 26. Circulation of streamwise vortices in the $k_x = 0$ modes for the flow of figure 25.

regeneration cycle. Since streak formation takes place during the decay of the vortex, the increase in circulation at the peak in $\Gamma_{k_x=0}$ increases circulation at subsequent times and simulates a delay in regeneration.

Two other cases of unsustained turbulence were examined, and the results, though not presented here, were consistent with the above: in both cases, decay of the turbulence could be prevented by increasing $\Gamma_{k_x=0}$ at an appropriate time before the final cycle. Though these four cases are insufficient to draw conclusions with any certainty, the results are suggestive. There are several ways to think about the effects of reducing the computational domain size below that required for sustained turbulence, but the most useful may be to think of the small domain as causing the flow to develop a very critical dependence on the time scales of each process in the regeneration cycle. As the domain becomes smaller, the streamwise vortices decay more quickly (Waleffe

1991) and the flow is less able to accommodate variation in the timing of breakdown and vortex regeneration. In the four cases of unsustained turbulence examined, the regeneration of streamwise vortices occurred with full vigour, but at the wrong times. Turbulence can be sustained only when streak formation, streak breakdown, and vortex regeneration occur at proper intervals, and it would appear that these intervals are incorrect for structures spaced more closely than the typically observed streak spacing.

We have only addressed the question of what factors determine the minimum spanwise streak spacing, but it seems reasonable to suspect that the maximum spacing may also be determined by the requirement for appropriately matched time scales of the regeneration processes. In a full-scale turbulent flow, structures may come into existence that have spanwise spacing larger or smaller than the expected value of about 100 ν/u_τ, but these structures will not be regenerated if the regeneration processes depend too critically on precise timing. Another possibility is as follows. The same sort of nonlinear interactions that regenerate the $(0,\beta)$-mode streamwise vortices also generate higher modes: $(0,2\beta)$, $(0,3\beta)$, etc. When β is based on a computational domain of $L_z^+ \approx 100$, the $(0,2\beta)$ mode cannot sustain a regeneration cycle of its own, as has been shown in this section. However, as L_z^+ approaches 200, the $(0,2\beta)$ mode can sustain the regeneration cycle, since this mode now corresponds to $\lambda_z^+ \approx 100$. The time scale of regeneration of the larger-scale (β) structures would be expected to be longer than for the smaller-scale (2β) structures (cf. figures 3 and 18, see also Butler & Farrell 1993 for the time scales of optimal perturbations with increasing spanwise wavelength), and the smaller-scale structures might dominate because they are regenerated faster. Simulations of a plane Couette flow with near minimum L_x and Reynolds number, but with L_z set to approximately twice the standard streak spacing, and initialized with random data develop two pairs of streamwise structures (i.e. $(0,2\beta)$ mode) with the correct spacing of $\lambda_z^+ \approx 100$. It has not been possible to determine what the role of the larger, $(0,\beta)$-mode, structures is in this evolution. Clearly, more study is needed to resolve the question of streak spacing.

The results of this section lend support the conjecture by Waleffe *et al.* (1993) that the minimum spanwise wavelength is set by the entire regeneration process, rather than any individual element of regeneration. When the computational domain is too narrow, turbulence decays because breakdown does not occur. Breakdown, in turn, depends on the creation of unstable streaks by sufficiently strong streamwise vortices. The strength of the streamwise vortices depends on vortex regeneration, and this, of course, returns us to the starting point, since regeneration depends on streak breakdown during the previous cycle.

8. Comparison with previous results

Streak formation by streamwise vortices has been well documented in the literature (e.g. Bakewell & Lumley 1967; Blackwelder & Eckelmann 1979; Landahl 1980), and the present findings are in agreement with previously published results. Streak breakdown has also received considerable attention in the literature, and it is generally found, as here, that streak instability is the cause of breakdown (e.g. Kim, Kline & Reynolds 1971; Swearingen & Blackwelder 1987). There is as yet, however, no general theory of the stability of three-dimensional flows, and the nature of the disturbances that might grow in a particular streaky flow is not easily determined. Streak formation and breakdown were included in the present study to help obtain an understanding of the regeneration of near-wall structures that is as complete and consistent as possible.

There is much less of a consensus regarding the origin of streamwise vortices in the near-wall region, and many possible mechanisms have been proposed. Jiménez & Moin (1991), in their study of a minimal plane Poiseuille flow, relied primarily on flow visualization to study the generation of streamwise vortices. They describe a mechanism in which regions of the spanwise vorticity associated with the mean flow tend to wrap around streamwise vortices, and in so doing, develop a wall-normal component of vorticity, ω_y. The shearing action of the mean flow then tilts this vorticity into the x-direction, producing streamwise vorticity, ω_x. Sendstad & Moin (1992), studying the same minimal plane Poiseuille flow, also found that the tilting of vorticity into the streamwise direction is the dominant mechanism for the generation of ω_x. Since the tilting of vorticity was found in the present study not to be the principal mechanism for regeneration of streamwise vortices, it is worthwhile to examine why these investigations differ.

The equation for the time evolution of streamwise vorticity may be written as

$$\frac{\partial \omega_x}{\partial t} = -\boldsymbol{u} \cdot \nabla \omega_x + \boldsymbol{\omega} \cdot \nabla u + \frac{1}{Re} \nabla^2 \omega_x \tag{8.1}$$

where the first term on the right side of the equation accounts for the redistribution of ω_x by advection, and the second term is, in effect, a source term for the creation of new ω_x within the bulk of the fluid. Sendstad & Moin (1992) were interested in the generation of streamwise vorticity in the near-wall region, and focused their attention on the source term. They found that the greatest contribution to $\boldsymbol{\omega} \cdot \nabla u$ was from the term

$$-\frac{\partial w}{\partial x} \frac{\partial u}{\partial y}. \tag{8.2}$$

They noted that the vorticity associated with this term forms in sheets which then roll up to become streamwise vortices. The $-(\partial w/\partial x)(\partial u/\partial y)$ term is the largest term, in physical space, in the present study as well. However, since streak formation requires streamwise vorticity in the $k_x = 0$ modes, it is important to ensure that any proposed mechanism for vortex regeneration produces these modes. Fourier decomposition of $-(\partial w/\partial x)(\partial u/\partial y)$ is plotted in figure 27. While there is some contribution to $\hat{\omega}_x(0, \beta)$ (heavy solid line), the greater contribution is to the $k_x = \alpha$ modes, and it has been shown (figure 7) that the $k_x = \alpha$ modes cannot, by themselves, produce the proper streaks. Instead, as discussed in §6, the regeneration cycle can only be closed by interactions among the α-modes that produce the elongated (x-independent) vortices that generate the observed streaks. The mechanism identified by Sendstad & Moin is an important one in the generation of these $k_x = \alpha$ modes, but is not sufficient to complete the regeneration cycle.

The Görtler-type, centrifugal instability and the related Craik–Leibovich instability have also been proposed for regeneration of streamwise vortices, as discussed in the Introduction. In the present flow, the curved pathlines required for Görtler vortices would be found only in the $k_x = \alpha$ and higher modes, and not in the $k_x = 0$ modes. Therefore, while streamwise vorticity might be produced by this mechanism, the modal interactions of §6 would still be required in order to produce elongated streamwise vortices and streaks. Of course, these instabilities can be important: in flow near a curved wall, say, for the case of the Görtler instability. But in that case the instability is imposed externally, and is not part of a self-regeneration cycle as discussed in this paper.

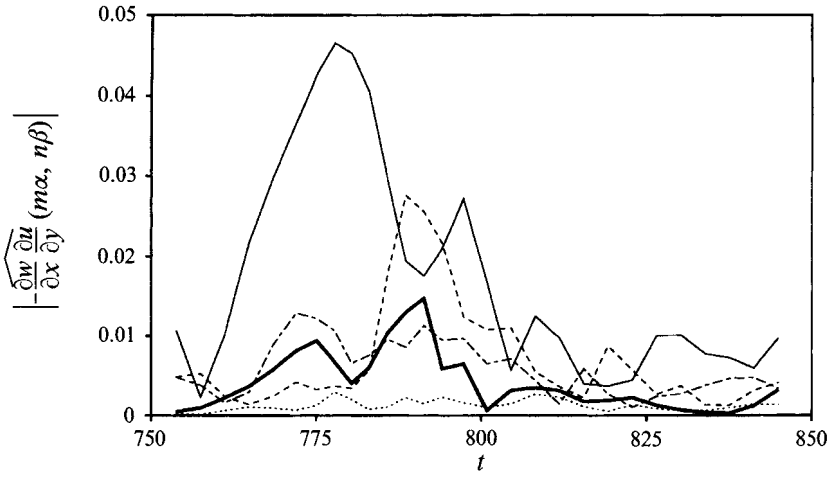

FIGURE 27. Fourier decomposition of $-(\partial w/\partial x)(\partial u/\partial y)$, integrated in y: ——— , $(0,\beta)$ mode; ····· , $(0,2\beta)$; ——— , $(\alpha,0)$; - - - - - - - , (α,β); - - - - - - - , $(\alpha,2\beta)$.

9. Discussion and conclusions

The research presented here was part of an attempt to understand the self-regeneration and the characteristic spanwise spacing of the structures commonly observed in the near-wall region of turbulent flows. The flow employed to study regeneration was a plane Couette flow with periodic streamwise and spanwise boundaries in which the Reynolds number, streamwise length, and spanwise width were near the minimum values required for turbulence to be sustained. This flow is ideal for the study of regeneration since it contains, by construction, the minimum set of structures required for sustained turbulence.

The turbulence structures in this minimal Couette flow were found to undergo a temporally quasi-cyclic process of regeneration, with little of the spatial randomness observed in full-scale turbulent flows. Each cycle consists of three, sequential sub-processes: streak formation, streak breakdown and vortex regeneration. The formation of streaks is found to be the result of simple advection of momentum by streamwise vortices, and breakdown is due to an instability of the streaks. During streak breakdown, a somewhat complicated set of interactions re-energizes the streamwise vortices, leading to formation of a new set of streaks, and completing the regeneration cycle. This process is illustrated schematically in figure 28.

The streamwise vortices in the near-wall region were found to account not only for the streaks, but also the general shape of the 'mean' (averaged in the x,z plane) velocity profile. This suggests the possibility that structure-based turbulence models may be able to adequately predict viscous drag by incorporating only the effect of the streamwise vortices and ignoring the other near-wall structures.

The vortex regeneration process was found to be somewhat complicated in the sense that the full increase in strength of the vortices could only be accounted for by including the nonlinear interactions of several pairs of spanwise Fourier modes. In addition, the distribution, in y, of the vorticity produced by these interactions varied widely for different modes and different terms in the vorticity equation. It is possible that vortex regeneration would prove less complicated if some appropriately chosen

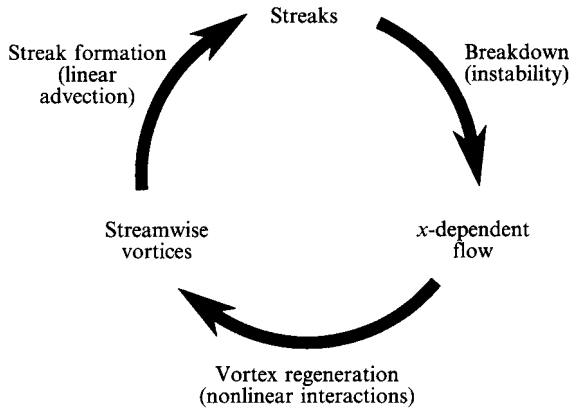

FIGURE 28. Schematic illustration of regeneration cycle of near-wall turbulence structures.

basis, other than Fourier modes, were used in the spanwise direction. This may be a useful approach for further study.

The flow used to study the streak spacing was similar to that used to study the regeneration process, except the dimensions of the computational domain were reduced below the values required to produce sustained turbulence. By reducing the spanwise dimension of the domain, we hoped to find which parts of the regeneration process were not sustained at short length scales, and thus why streak spacings of less than about 100 ν/u_τ are not observed. Four realizations of unsustained turbulence were examined, and, in each case, we found that all the regeneration mechanisms continue to function, up to a point. It appears, however, that a mismatch develops in the timing of the processes and interrupts the regeneration cycle. Such a mismatch might also occur at larger length scales, explaining why a dominant streak spacing of 100 ν/u_τ is observed, but this was not examined in the present work.

The results of the streak spacing investigation also give support the conjecture by Waleffe *et al.* (1993) that streak spacing is set by the entire regeneration process, rather than by any single component of the process (such as streak formation).

Perhaps the most interesting aspect of the regeneration cycle described here is that it is a cycle, and breaking the cycle at any point would prevent regeneration of new near-wall structures. Since, as discussed earlier, turbulence cannot be maintained without the near-wall structures (Jiménez & Moin 1991), designing flow modifications to break or partially disrupt the regeneration cycle may be an ideal way to approach turbulent drag reduction or control.

The highly constrained flow studied here was chosen as ideal for an attempt to discover which processes are important in the regeneration of near-wall structures. It remains to be seen to what extent the mechanisms identified here carry over into full-scale turbulent flows. Real turbulence, of course, is not periodic in x and z, and Fourier decomposition is of less use in isolating structures and their dynamics. The regeneration mechanisms identified here, however, all have physical space interpretations, and it is important that comparisons be made to unconstrained turbulent flows.

REFERENCES

AUBRY, N., HOLMES, P., LUMLEY, J. L. & STONE, E. 1988 The dynamics of coherent structures in the wall region of a turbulent boundary layer. *J. Fluid Mech.* **192**, 115–173.

BAKEWELL, H. P. & LUMLEY, J. L. 1967 Viscous sublayer and adjacent wall region in turbulent pipe flow. *Phys. Fluids* **10**, 1880–1889.

BLACKWELDER, R. F. & ECKELMANN, H. 1979 Streamwise vortices associated with the bursting phenomenon. *J. Fluid Mech.* **94**, 577–594.

BUTLER, K. M. & FARRELL, B. F. 1993 Optimal perturbations and streak spacing in wall-bounded turbulent shear flow. *Phys. Fluids* A **5**, 774–777.

COLES, D. 1978 A model for flow in the viscous sublayer. In *Workshop on Coherent Structure of Turbulent Boundary Layers* (ed. C. R. Smith & D. E. Abbott), pp. 462–475. Lehigh University.

CRAIK, A. D. D. 1982 Wave-induced longitudinal-vortex instability in shear flows. *J. Fluid Mech.* **125**, 37–52.

CRAIK, A. D. D. & LEIBOVICH, S. 1976 A rational model for Langmuir circulations. *J. Fluid Mech.* **73**, 401–426.

ELLINGSEN, T. & PALM, E. 1975 Stability of linear flow. *Phys. Fluids* **18**, 487–488.

HAMILTON, J. M. & ABERNATHY, F. H. 1994 Streamwise vortices and transition to turbulence. *J. Fluid Mech.* **264**, 185–212.

JANG, P. S., BENNEY, D. J. & GRAN, R. L. 1986 On the origin of streamwise vortices in a turbulent boundary layer. *J. Fluid Mech.* **169**, 109–123.

JIMÉNEZ, J. 1994 On the structure and control of near wall turbulence. *Phys. Fluids* **6**, 944–953.

JIMÉNEZ, J. & MOIN, P. 1991 The minimal flow unit in near-wall turbulence. *J. Fluid Mech.* **225**, 213–240.

KIM, H. T., KLINE, S. J. & REYNOLDS, W. C. 1971 The production of turbulence near a smooth wall in a turbulent boundary layer. *J. Fluid Mech.* **50**, 133–160.

KIM, J., MOIN, P. & MOSER, R. 1987 Turbulence statistics in fully developed channel flow at low Reynolds number. *J. Fluid Mech.* **177**, 133–166.

KLEBANOFF, P. S., TIDSTROM, K. D. & SARGENT, L. M. 1962 The three-dimensional nature of boundary-layer instability. *J. Fluid Mech.* **12**, 1–34.

KLINE, S. J., REYNOLDS, W. C., SCHRAUB, F. A. & RUNDSTADLER, P. W. 1967 The structure of turbulent boundary layers. *J. Fluid Mech.* **30**, 741–773.

LANDAHL, M. T. 1980 A note on an algebraic instability of inviscid parallel shear flows. *J. Fluid Mech.* **98**, 243–251.

ROBINSON, S. K. 1991 The kinematics of turbulent boundary layer structure. *NASA TM* 103859.

SENDSTAD, O. & MOIN, P. 1992 The near wall mechanics of three-dimensional turbulent boundary layers. *Rep.* TF-57. Department of Mechanical Engineering, Stanford University, Stanford, California, USA.

SMITH, C. R. & METZLER, S. P. 1983 The characteristics of low-speed streaks in the near-wall region of a turbulent boundary layer. *J. Fluid Mech.* **129**, 27–54.

SREENIVASAN, K. R. 1988 A unified view of the origin and morphology of the turbulent boundary layer structure. In *Turbulence Management and Relaminarisation: Proc. IUTAM Symp. on Turbulence Management and Relaminarisation* (ed. H. W. Liepmann & R. Narasimha), pp. 37–61. Springer.

SWEARINGEN, J. D. & BLACKWELDER, R. F. 1987 The growth and breakdown of streamwise vortices in the presence of a wall. *J. Fluid Mech.* **182**, 255–290.

WALEFFE, F. 1991 On the origin of the streak spacing in turbulent shear flows. In *Annual Research Briefs–1990*. Center for Turbulence Research, Stanford Univ./NASA-Ames, pp. 159–168.

WALEFFE, F., KIM, J. & HAMILTON, J. M. 1993 On the origin of streaks in turbulent boundary layers. In *Turbulent Shear Flows 8* (ed. F. Durst, R. Friedrich, B. E. Launder, F. W. Schmidt, U. Schumann, J. H. Whitelaw), pp. 37–49. Springer.